Geochemistry, Geophysics, Geosystems

RESEARCH ARTICLE
10.1029/2020GC009334

# Estimates of the Temperature and Melting Conditions of the Carpathian-Pannonian Upper Mantle From Volcanism and Seismology

**Antoine J. J. Bracco Gartner**[1] **and Dan McKenzie**[2]

[1]Faculty of Science, Vrije Universiteit Amsterdam, Amsterdam, The Netherlands, [2]Bullard Laboratories, Department of Earth Sciences, University of Cambridge, Cambridge, UK

**Key Points:**
- Carpathian-Pannonian intraplate basalts are formed by less than 1% melting in the garnet-spinel transition zone, at depths of about 63–72 km
- The calculated melt distributions correspond to a mantle potential temperature of 1257°C beneath the Pannonian Basin
- Melting occurs because the base of the lithosphere (at about 1300°C) is close to the solidus temperature over a large part of the Basin

**Supporting Information:**
- Supporting Information S1

**Correspondence to:**
A. J. J. Bracco Gartner,
a.j.j.braccogartner@vu.nl

**Citation:**
Bracco Gartner, A. J. J., & McKenzie, D. (2020). Estimates of the temperature and melting conditions of the Carpathian-Pannonian upper mantle from volcanism and seismology. *Geochemistry, Geophysics, Geosystems*, *21*, e2020GC009334. https://doi.org/10.1029/2020GC009334

Received 30 JUL 2020
Accepted 11 SEP 2020
Accepted article online 16 SEP 2020



**Abstract** What drives the formation of basaltic melts beneath intraplate volcanoes not associated with extensive thermal anomalies or lithospheric extension? Detailed constraints on the melting conditions and source region are imperative to resolve this question. Here we model the geochemistry of alkali basalts and mantle nodules brought up by young (12–0.1 Ma) intraplate volcanoes distributed across the Carpathian-Pannonian region and combine the results with geophysical observations. Rare earth element inversion and forward calculation of elemental concentrations show that the basalts require the mantle to have undergone less than 1% melting in the garnet-spinel transition zone, at depths of about 63–72 km. The calculated melt distributions correspond to a mantle potential temperature of ~1257°C, equivalent to a real temperature of 1290°C at 65 km beneath the Pannonian Basin. The composition, modal mineralogy, and clinopyroxene geochemistry of some of the entrained mantle nodules closely resemble the basalt source, though the latter equilibrated at greater depths. The gravity anomalies and topography of the Basin reveal no large-scale features that can account for the post-extensional volcanism. Instead, the lithospheric thickness and geotherm show that melting occurs because the base of the lithosphere, at ~50-km depth, is close to or at the solidus temperature over a large part of the Basin. Hence, only a small amount of upwelling is required to produce minor volumes (up to a few cubic kilometers) of melt. We conclude that the Pannonian volcanism originates from upwelling in the asthenosphere just below thinned lithosphere, which is likely to be driven by thermal buoyancy.

**Plain Language Summary** On Earth's continents, there are surprising instances of basaltic volcanism that are not related to plate stretching or hotspots. To understand just such activity in the Carpathian-Pannonian region, in eastern central Europe, during the last 12 million years, we studied the chemical composition of the erupted lavas. Using a computer code that takes as input the concentrations of elements in basaltic rocks, we calculated the fraction of melt and the depth at which it formed within Earth's mantle. We find that the mantle has undergone less than 1% melting in the garnet-spinel transition zone—a region at about 63- to 72-km depth where these minerals both occur. Using a model of mantle melting, we find that the temperature of the mantle at 65 km below the Pannonian Basin is about 1290°C. The plate's thickness and the temperature variations with depth tell us that the magma source region is at a temperature close to that at which melting begins (the solidus). This means that if mantle material is moved upwards just slightly, it will produce small volumes of melt that can rise to the surface. The most likely cause of such upward movement is convection in the mantle below the rigid plate.

## 1. Introduction

The processes that govern the formation of minor volumes of basalts away from active plate boundaries are subject to widespread debate. Although such rocks exhibit geochemical signatures similar to ocean-island basalts (OIBs) and continental flood basalts—both considered the products of upwelling mantle plumes (e.g., Morgan, 1971; Richards et al., 1989; White & McKenzie, 1995)—it is increasingly evident that many instances of small-volume intraplate volcanism may not be driven by deeply sourced excess heat as originally hypothesized (e.g., Foulger & Natland, 2003). Numerous conceptual mechanisms have been proposed to explain such small-volume occurrences. These often involve some form of plate tectonic control, wherein lithospheric extension allows melts to rise to the surface (e.g., Foulger & Natland, 2003), or sublithospheric

processes, such as edge-driven convection (King & Anderson, 1995, 1998; King & Ritsema, 2000), shear-driven upwelling (Conrad et al., 2010), small-scale convection (Ballmer et al., 2007), or hydrous upwellings (Long et al., 2019; Yang & Faccenda, 2020). The ubiquity and viability of many such driving forces, however, remain contentious.

To determine whether intraplate magma generation is driven by the plate above or by processes below requires an integrated set of observations. Particularly valuable insights are contained in basaltic lavas, whose geochemistry and volume provide a record of the chemical, thermal, and dynamical state of their mantle source regions (e.g., Brown & Lesher, 2016; Ghiorso et al., 2002; McKenzie & O'Nions, 1991; Plank & Forsyth, 2016). Because their compositions reflect the composition and mineralogy of the source, the depth and degree of melting, and the temperature distribution in the mantle, they can be used to probe the physical processes in, and properties of, the melt source. These geochemical observables, used as key input for models of mantle melting, coupled with geophysical signals observable at the Earth's surface, such as gravity anomalies, surface wave velocities, and topography, allow holistic constraints to be placed on the origin of intraplate volcanism (e.g., Ball et al., 2019; Klöcking et al., 2018; McNab et al., 2018).

A region whose intraplate volcanism is not well understood is that of the Pannonian Basin and Carpathians in eastern central Europe. Dispersed throughout this area, small volumes of alkali basalts were erupted over the last 12 million years (Embey-Isztin, Downes, et al., 1993; Seghedi et al., 2004). The surprising feature of this continental volcanism is that it largely postdates the extension in the Pannonian Basin, which had ceased by the Late Miocene (Horváth et al., 2015). Consequently, a variety of causes has been proposed to explain the generation of basaltic melts. These include decompression melting by asthenospheric upwelling, "finger-like" asthenospheric plumes, lithospheric edge-related mantle flow, plate tectonic processes (Embey-Isztin, Downes, et al., 1993, 2001; Harangi et al., 2015; Seghedi et al., 2004, 2011; Wilson & Downes, 1991), and mantle water content and compression (Kovács et al., 2020). To understand the nature of this post-extensional intraplate volcanism, as well as similar instances worldwide, it is clearly desirable to obtain robust constraints on the generation of melt and its source region.

Here we present the results of melting models based on a judiciously screened geochemical data set of the most primitive erupted products of young intraplate magmatism in the Carpathian-Pannonian region. First, rare earth element (REE) inversion and forward element modeling are employed to determine the nature of the melt source and estimate the melting depth and melt fractions involved. Using the calculated melt distributions and a parameterization of mantle melting, we quantify the mantle potential temperature ($T_P$) beneath the Pannonian Basin. The calculated composition and mineralogy of the source region is then compared to that of the mantle nodules brought up by the basalts, in order to assess whether these may represent fragments of basalt source rock. Lastly, we examine the geophysical features of the Basin and place integrated constraints on the origin of intraplate volcanism in the region.

## 2. Geological Setting

### 2.1. Carpathian-Pannonian Geodynamics

The Pannonian Basin is a major extensional basin located in eastern central Europe and constitutes part of the Alpine-Mediterranean orogenic system (Horváth et al., 2006; Royden, 1988). It is surrounded by the arcuate Carpathian orogen to the north, east, and south and the Eastern Alps and Dinarides to the west (Figures 1 and 2). The Basin is a result of E-W-directed extension during the Miocene, which started at ca. 20 Ma and continued until 8–9 Ma, with peak rates around 11–15 Ma (Balázs et al., 2016, 2017; Horváth et al., 2006). This extension was largely coeval with, and of similar magnitude to, the shortening recorded in the outer Carpathians (Horváth et al., 2015). A 2–5 km thick sequence of Miocene sediments was deposited in the Basin during this period, predominantly onto the deformed Cretaceous–Paleogene rock units of the AlCaPa and Tisza-Dacia microplates (Balázs et al., 2017; Horváth et al., 2006; Schmid et al., 2020). The regional stretching was accompanied by severe attenuation of the lithosphere, and as a result, the Basin is presently underlain by a thin continental lithosphere (~50 km; Figure 1b), of which the upper 21–35 km is crust (Horváth et al., 2006; Priestley et al., 2018).

Miocene extension is generally considered to have resulted from rollback of the subducting lithospheric slab and resulting "back-arc" formation in the Basin (Balázs et al., 2016; Horváth et al., 2006; Royden, 1988; Ustaszewski et al., 2008). Cessation of extension was followed by basin inversion since the Late Miocene

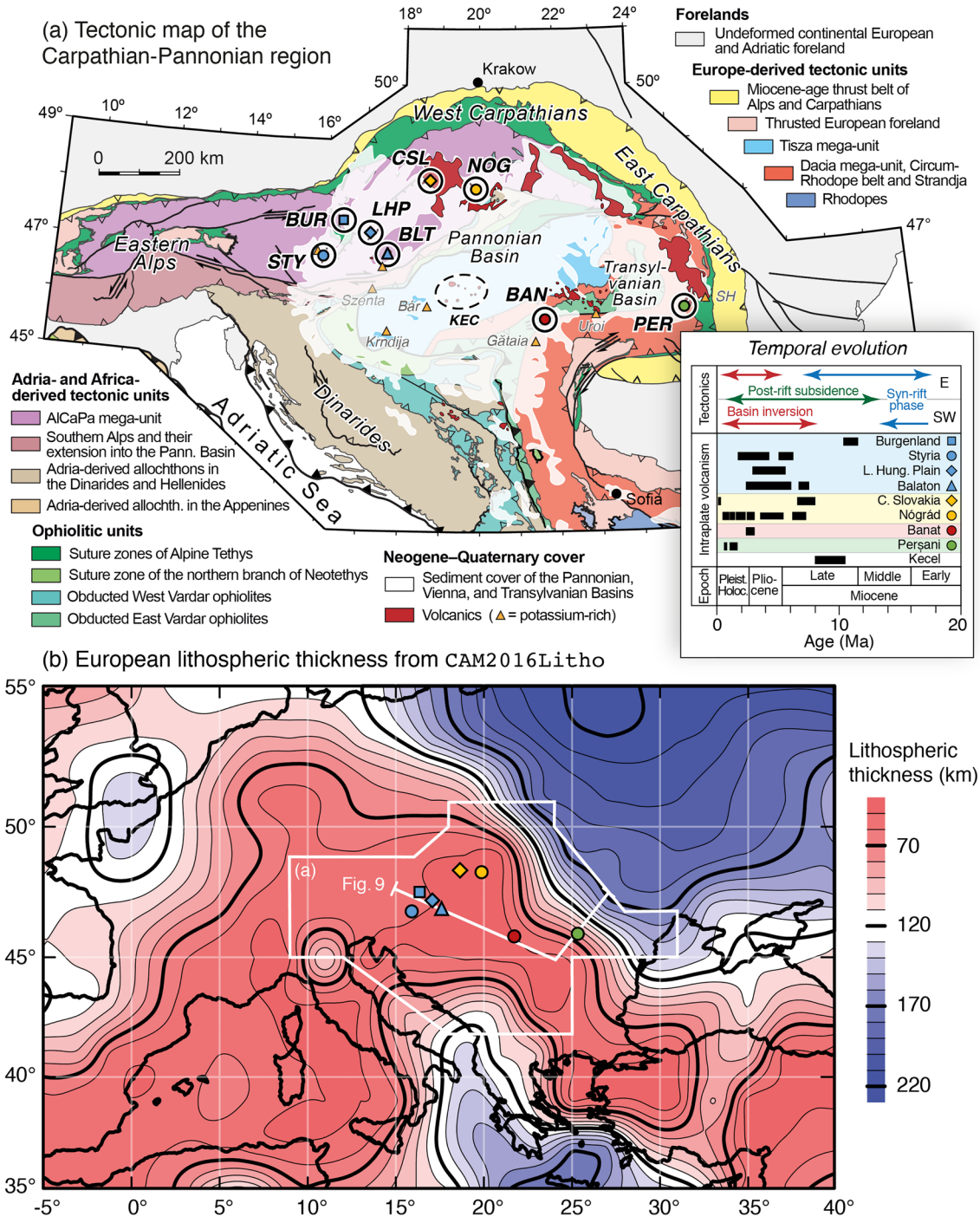


**Figure 1.** (a) Tectonic map of the Carpathian-Pannonian region (Schmid et al., 2020) with its Neogene-Quaternary volcanic and sedimentary cover (Horváth et al., 2015). The studied intraplate volcanic fields are labeled STY (Styria), BUR (Burgenland), LHP (Little Hungarian Plain), BLT (Balaton), CSL (Central Slovakia), NOG (Nógrád), BAN (Banat), and PER (Perşani). KEC = Kecel (buried basalts), SH = Southern Harghita. Orange triangles indicate potassium-rich volcanic rocks. Inset shows the temporal evolution of regional intraplate volcanism and tectonics (compiled from Balázs et al., 2016; Seghedi et al., 2004; and references therein). (b) Mercator projection map of lithospheric thickness in Europe from CAM2016Litho (IRIS, 2018), calculated from surface wave tomography (see main text; Priestley et al., 2018). Shown are the sample locations, approximate outline of the map in (a), and profile trace of Figure 9.

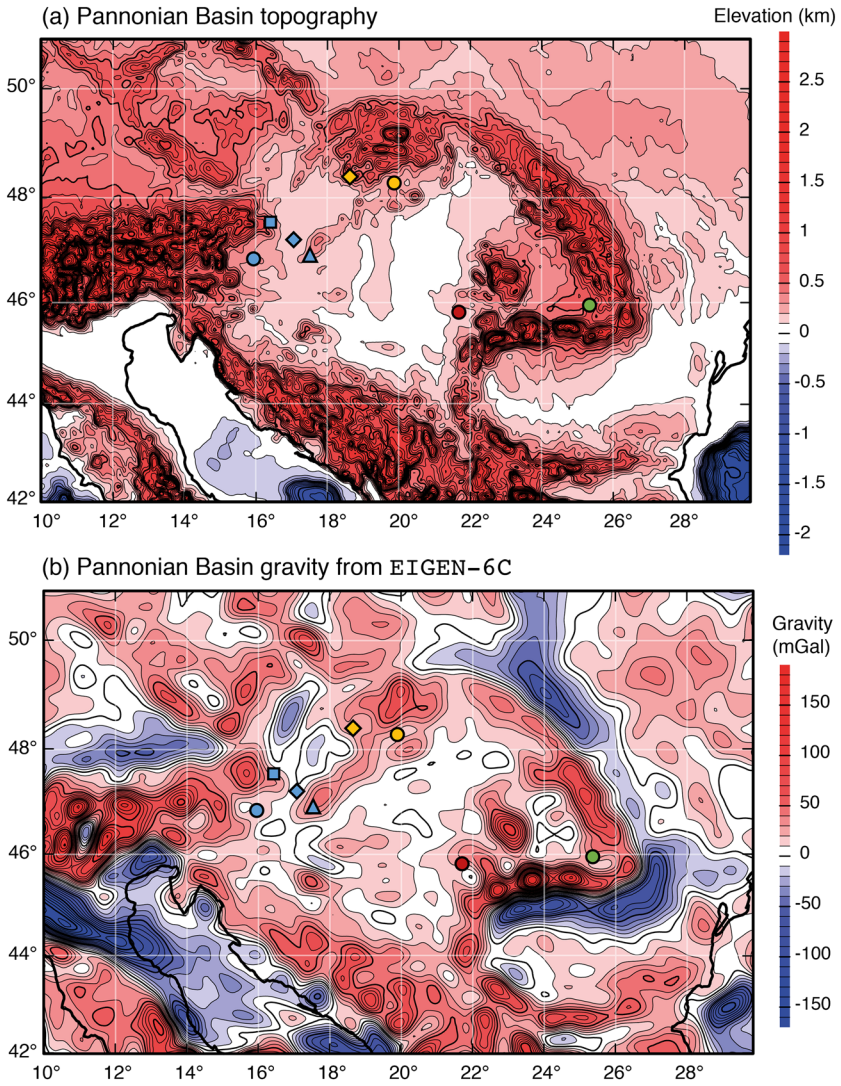


**Figure 2.** (a) Topography of the Carpathian-Pannonian region from the Global Topography 1-min grid (Smith & Sandwell, 1997) (available from https://topex.ucsd.edu/marine_topo/, version 19.1), smoothed to remove wavelengths less than 20 km. (b) Gravity field from the EIGEN-6C global combined gravity field model (Förste et al., 2014; Shako et al., 2014) (available from https://doi.org/10.5880/icgem.2015.1), filtered to remove anomalies whose horizontal wavelength is less than 60 km. Both panels are Mercator projection maps. Sample locations and symbols of intraplate volcanics as in Figure 1.

(inset Figure 1a), perhaps as a response to the counterclockwise rotation and NNE-directed indentation of the Adriatic microplate (Balázs et al., 2016; Dombrádi et al., 2010; Horváth et al., 2015). Active seismicity presently occurs beneath Vrancea in the southern East Carpathians, where it is associated with a near-vertical slab still attached to the surface (e.g., Martin & Wenzel, 2006). The other lithospheric slabs that were previously subducted along the Carpathian arc have already been detached: their remnants are imaged at depths of 410–660 km by seismic tomography (Wortel & Spakman, 2000).

### 2.2. Intraplate Volcanism

The Carpathian-Pannonian region is marked by episodic intracontinental volcanism during Middle Miocene to Quaternary times. Its products are alkali basalts and rare potassium-rich lavas, which collectively amount to a few cubic kilometers. The eruptions generally postdate the subduction-related calc-alkaline magmatism of the inner Carpathians and Pannonian Basin and are dispersed both in space and time (Pécskay et al., 2006; Seghedi et al., 2004) (Figure 1a). Suites of alkali basalts are found in the volcanic fields of Styria ("Graz Basin"), Balaton ("Bakony-Balaton Highland"), Nógrád ("Nógrád-Gömör" or "Novohrad-Gemer"), and

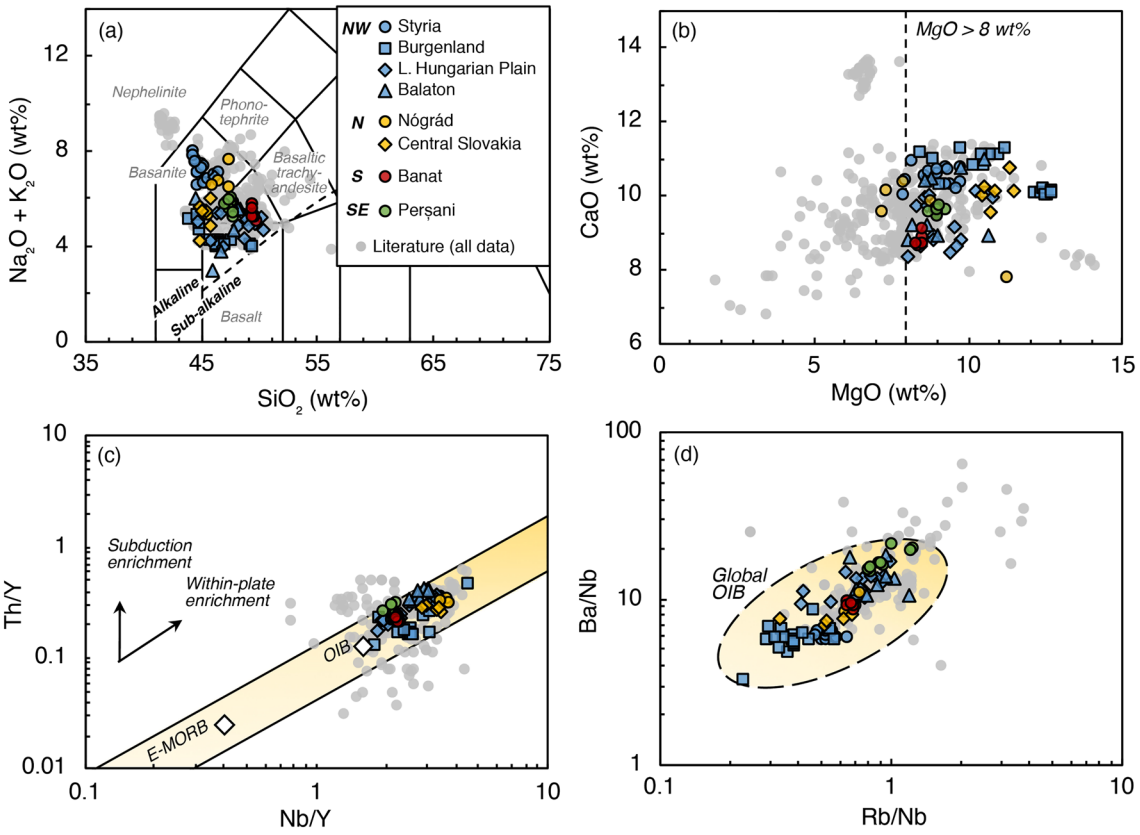


**Figure 3.** Major and trace element compositions of the alkali basalts from the Carpathian-Pannonian region. (a) $SiO_2$ versus total alkali ($Na_2O + K_2O$; wt%) classification diagram (Le Bas et al., 1986). Boundary between alkaline and subalkaline fields after Miyashiro (1978). (b) MgO versus CaO content (wt%). Major element oxide concentrations were normalized to 100 wt% on a volatile-free basis. (c) Nb/Y versus Th/Y, with mantle array and lines with arrows indicating directions of subduction and within-plate enrichment (Pearce & Peate, 1995; Sun & McDonough, 1989). Average compositions of ocean-island basalt (OIB) and enriched mid-ocean ridge basalt (E-MORB) are from Sun and McDonough (1989). (d) Rb/Nb versus Ba/Nb, with a global suite of OIBs (Willbold & Stracke, 2006). The colored data (symbols as in Figure 1) are those selected according to the screening criteria outlined in the main text. Published whole-rock data (Ali & Ntaflos, 2011; Ali et al., 2013; Dobosi & Jenner, 1999; Dobosi et al., 1995; Downes et al., 1995; Ducea et al., 2020; Embey-Isztin, Dobosi, et al., 1993; Embey-Isztin, Downes, et al., 1993; Harangi et al., 1994, 2013, 2015; Harangi, Vaselli, et al., 1995; Ivan & Hovorka, 1993; Jankovics et al., 2015, 2019; Rosenbaum et al., 1997; Tschegg et al., 2010) are listed in the supporting information.

Perşani, and at the local eruptive centers of Burgenland, Little Hungarian Plain, Banat ("Lucareţ"), and Central Slovakia ("Štiavnica") (e.g., Embey-Isztin, Downes, et al., 1993; Harangi et al., 2015; Seghedi et al., 2004). Boreholes in the center of the Basin, near Kecel (Figure 1a), have further revealed various alkali basalts of Late Miocene age (8–11 Ma) buried beneath sediments (Seghedi et al., 2004, and references therein), but no detailed petrological data are yet available from these basalts. Indeed, seismic sections, boreholes, and gravity and magnetic anomaly data concerned with the interior of the Basin (e.g., Zelenka et al., 2004) suggest that similar rocks have been buried by sedimentation in those parts that experienced rapid subsidence. Hence, the present-day surface distribution of the basalts is probably biased toward the margins of the Basin and toward relatively young occurrences.

The petrological features of the exposed rocks and their nodules have been widely documented (e.g., Embey-Isztin, Downes, et al., 1993; Harangi et al., 2015; Seghedi et al., 2004; Szabó et al., 2004; Vaselli et al., 1995). The erupted rocks are mostly alkali basalts, trachybasalts, basanites, and rare nephelinites (Figure 3a), which contain phenocrysts of olivine (±spinel inclusions) ± clinopyroxene (Embey-Isztin, Downes, et al., 1993). They are silica undersaturated, have high MgO contents (up to 14 wt%; Figure 3b), and generally display only modest effects of fractional crystallization (Harangi et al., 2015). Their trace element compositions resemble those typically observed in OIBs (Figures 3 and 4), and their radiogenic isotope ratios display similarities with contemporaneous mafic alkaline rocks in western central Europe (Wilson & Downes, 1991). Petrological studies indicate that the melts parental to the basalts were principally

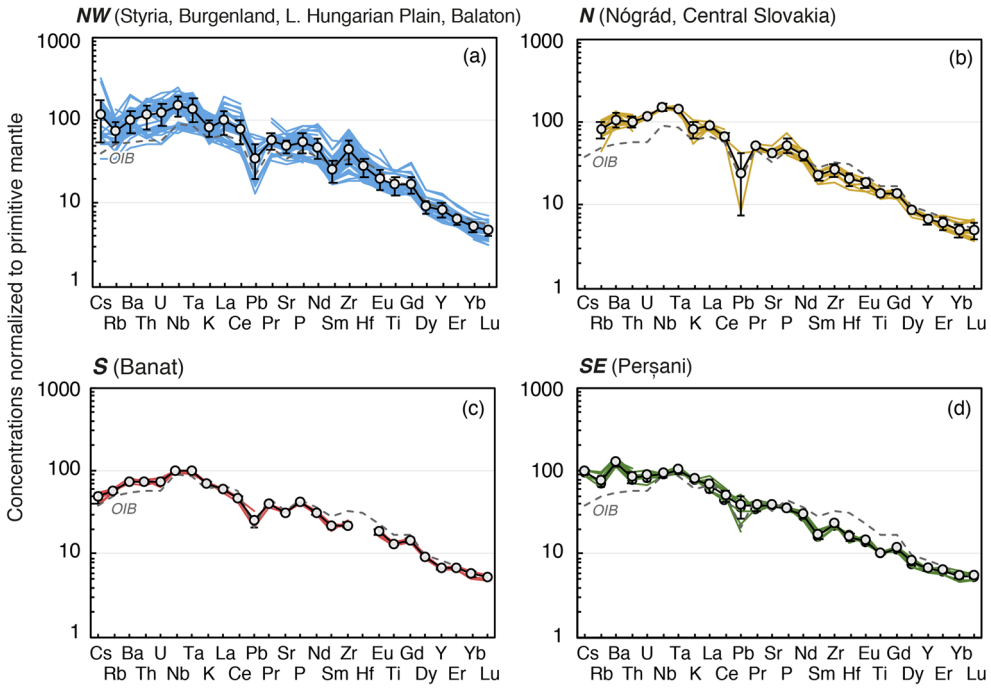


**Figure 4.** Trace element patterns of the screened alkali basalts from the (a) NW (Balaton, Little Hungarian Plain, Styria, and Burgenland), (b) N (Nógrád and Central Slovakia), (c) S (Banat), and (d) SE (Perşani). Black lines with circles are the average compositions ±1 SD. Concentrations are normalized to those in the primitive mantle (McKenzie & O'Nions, 1991, 1995). Average composition of ocean-island basalt (OIB; grey dashed line) is from Sun and McDonough (1989). Data sources as in Figure 3.

sourced from the asthenosphere and that some were modified by interaction with the lithospheric mantle during ascent (Embey-Isztin, Downes, et al., 1993; Harangi et al., 2015; Seghedi et al., 2004). Trace element concentrations in melt inclusions in olivines from Perşani show averages that coincide with whole-rock data (Bracco Gartner et al., 2020), demonstrating that (near-)primary melt characteristics were largely preserved in the bulk lavas.

Intraplate volcanism was accompanied by sporadic eruptions of low-volume, potassium-rich products during the Middle Miocene (13–16 Ma) and Quaternary (0.9–2.2 Ma) (Harangi, Wilson, et al., 1995; Seghedi et al., 2004, 2011). These are shown as orange triangles in Figure 1a. Those of Middle Miocene age occur close to where the alkali basalts of Styria and Balaton would later erupt. The Quaternary occurrences are found more dispersed throughout the Basin, near Bár, Gătaia, Uroi, and in Southern Harghita. These potassic melts seem to record a signature of lithospheric domains previously metasomatized by subduction-related agents (e.g., Harangi, Wilson, et al., 1995; Seghedi et al., 2011) and are likely to be of shallower origin than the alkali basalts.

## 3. Methods

### 3.1. Sample Selection

An important prerequisite for the present study is the selection of rock samples that most closely reflect the composition of their respective primary magmas. Hence, judicious screening is required to mitigate the effects of processes such as fractional crystallization and lithospheric/crustal contamination, which confuse the relationship between erupted products and their primary melts. To identify and account for these effects, detailed major and trace element analyses are required. Hence, the synthesized data set includes only those samples for which both are analyzed and are sufficiently precise.

The assembled data set comprises major and trace element and, where available, radiogenic isotope analyses for the most primitive alkali basalts from all exposed volcanic districts (supporting information; Figure 3). The least-evolved and least-fractionated rocks were selected by adopting cut-off values of $SiO_2 \leq 50$ wt% (Figure 3a) and $MgO \geq 8$ wt% (Figure 3b), which ensure that olivine was the dominant fractionating

phase. A cautious exception was made for Nógrád (MgO ≥ 7.3 wt%, whose trace element concentrations closely resemble the less-fractionated samples), in order to yield a greater data set. Lack of correlation between light-over-middle REEs such as La/Sm, which are known to increase during extensive clinopyroxene crystallization, and indicators of clinopyroxene crystallization (e.g., Sc/Y and Ca/Al), demonstrate that this process did not strongly affect the screened samples. Trace element ratios were employed to identify OIB-like samples and discard those which show evidence of secondary modification or interaction with lithospheric and/or metasomatized domains. The selected samples plot on the mantle array in Nb/Y–Th/Y space (Pearce & Peate, 1995) (Figure 3c) and within the field of global OIBs in Rb/Nb–Ba/Nb space (Willbold & Stracke, 2006) (Figure 3d).

The basalts are grouped into four suites corresponding to the locations in Figure 1: NW (Styria, Burgenland, Little Hungarian Plain, and Balaton), N (Central Slovakia and Nógrád), S (Banat), and SE (Perşani). Their primitive mantle-normalized incompatible element patterns and calculated averages (±1 standard deviation [SD]) are shown in Figure 4.

### 3.2. Melting Model and Application

Relative abundances of incompatible elements allow quantitative constraints to be placed on the conditions of primary melt generation (McKenzie & O'Nions, 1991, 1995). Owing to their inter-elemental differences in compatibility, REEs are particularly sensitive to the cumulative amount of melting and the relative proportion of melting in the garnet and spinel stability fields. Assuming that the melt source is homogeneous and the resulting basalt is a homogeneous mixture of the fractional melts, REEs can be used to determine the depth of the melting interval and the melt fraction involved. The best-fitting solution can be sought iteratively by employing computational inversion, such as performed by the `INVMEL` (inversion melting) algorithm. This scheme inverts observed REE concentrations for the best-fitting melt distribution as a monotonic function of depth for a specified source composition (see McKenzie & O'Nions, 1991, 1995, for the original version and theoretical basis). For a given inversion, the melting depth interval, the top of the melting column, and initial distribution of melt fraction with depth are varied iteratively, and fractional melts are summed over incremental depths. The minimum root mean square misfit ($M$) between the observed ($c_i^o$) and calculated concentration ratios ($c_i^c$) of the REEs (elements $i$) is sought using Powell's conjugate direction method. $M$ is defined as

$$M = \left[\frac{1}{N}\sum_{i=1}^{N}\frac{(c_i^o - c_i^c)^2}{\sigma_i{}^2}\right]^{1/2} \quad (1)$$

where $N$ is the number of REEs and $\sigma_i$ is the SD. Once the optimal solution is obtained, the forward model calculates concentrations of other elements by integrating instantaneous fractional melts over incremental depths. Comparison of the calculated and observed concentrations of elements other than the REEs provides an independent test of the melting model obtained from the inversion.

`INVMEL` exploits a consistent set of mineral-melt REE partition coefficients determined by lattice strain parameterization (Blundy & Wood, 1994; Brice, 1975; Wood & Blundy, 1997). Details of these calculations for the REEs, as well as the partition coefficients for all elements used in the modeling, are provided in Appendix A and the supporting information, respectively. The effects of temperature and phase composition on these values are small relative to the other uncertainties inherent to the modeling (McKenzie & Blundy, 1999).

The composition of the melt source region was gauged by the observed Nd isotopic ratios ($\epsilon_{Nd}$ values) of the screened samples (following White & McKenzie, 1995). The average value of $\epsilon_{Nd}$ for all the basalts discussed here is 3.3. The composition of the source model used for modeling was therefore calculated by combining the primitive source of McKenzie and O'Nions (1991, 1995), with $\epsilon_{Nd} = 0$, and their MORB source, with $\epsilon_{Nd} = 10$, in appropriate fractions to generate a source with $\epsilon_{Nd} = 3.3$. The composition of this source, here termed Pannonian Upper MAntle (PUMA), is tabulated in the supporting information. The modal mineralogy corresponding to a source with this bulk composition is $Ol_{0.58}Opx_{0.27}Cpx_{0.12}Sp_{0.03}$ (in the spinel peridotite field) and $Ol_{0.62}Opx_{0.14}Cpx_{0.11}Gt_{0.13}$ (in the garnet peridotite field).

The calculated depth of melting is principally governed by the depth of the phase change from spinel to garnet peridotite. Experimental studies have shown that this transition is sensitive to temperature

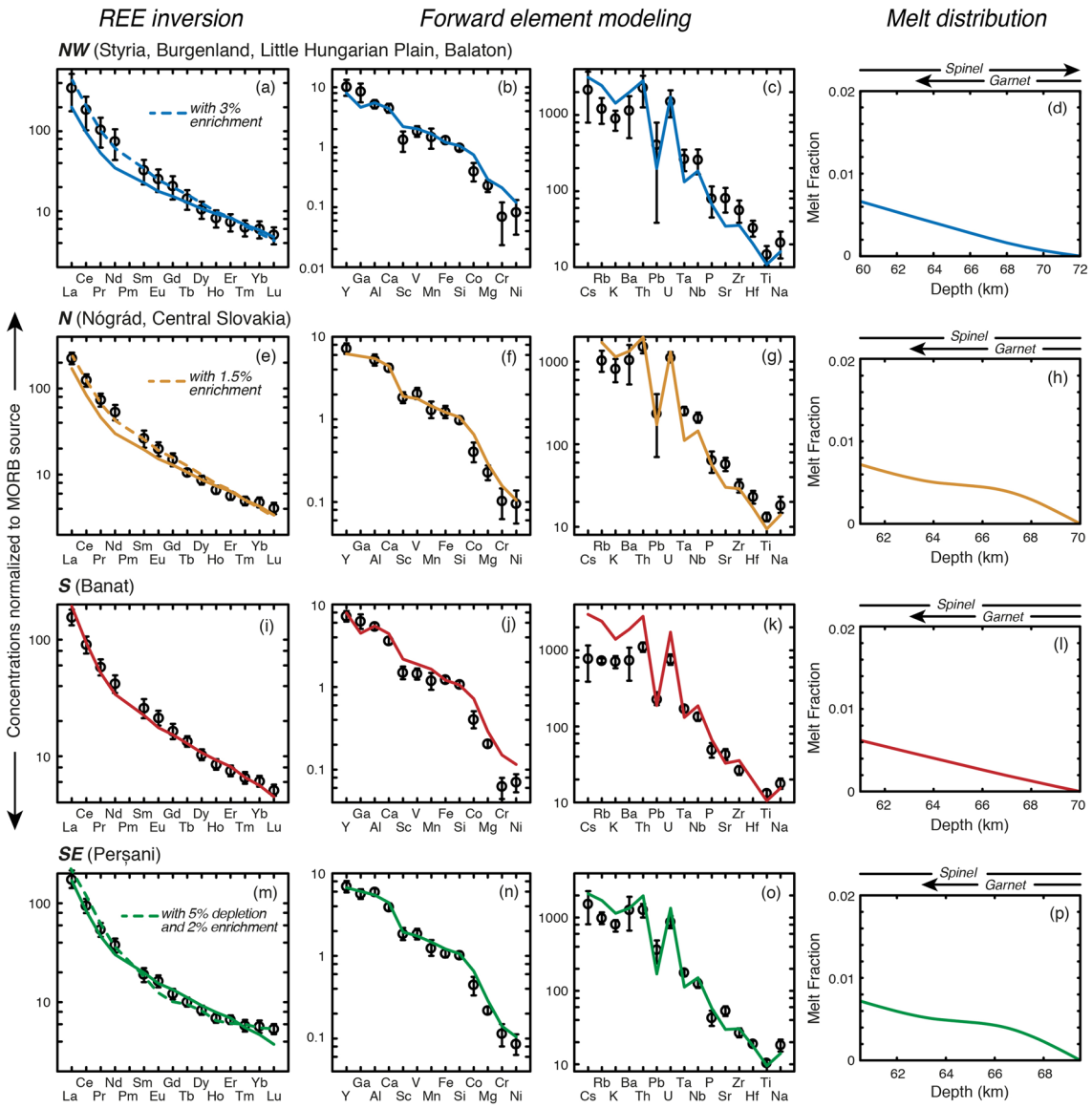


**Figure 5.** Inverse and forward element modeling of the elemental compositions of the Carpathian-Pannonian alkali basalts. (a, e, i, m) Rare earth element (REE) concentrations, which were used in the inversion. Black circles with error bars indicate the average observed concentrations ±1 SD. Solid lines represent the best-fitting REE distributions as calculated by the inversion. Dashed lines illustrate the fits that can be obtained using a multistage melting model as discussed in the main text. (b, f, j, n) Trace and (c, g, k, o) major and minor element concentrations, which were used in the forward model. Here, solid lines represent the calculated concentration ratios. All concentrations are normalized to the MORB source of McKenzie and O'Nions (1991, 1995). The standard deviation was calculated by combining the standard deviation of the observed concentrations and the uncertainties in the PUMA source concentrations. (d, h, l, p) Melt fraction as a function of depth. Solid lines indicate the calculated melt distributions. Those in (d) and (l) are isentropic, and those in (h) and (p) are the best fits from the inversion. Lines with arrows above the plots indicate the depths of garnet and spinel stability.

(Klemme & O'Neill, 2000). Based on their laboratory experiments, Klemme and O'Neill (2000) proposed that this transition occurred between 60 and 80 km for a $T_P$ of 1315°C. Thermodynamic modeling by Jennings and Holland (2015), however, suggests that the pressure of the garnet-spinel transition was previously overestimated due to the simplicity of the phase assemblage considered (i.e., Mg-Al-Si without Ca). These authors allowed for the activity of Ca in garnet and show that the transition intersects the solidus at 2.14–2.17 GPa. We used 63–72 km (2.1–2.4 GPa) for the transition from spinel to garnet peridotite.

The calculated MgO concentrations in the basalts were all greater than 8 wt% and were used to estimate the fraction of olivine that was removed from the magmas by crystallization. This was done by comparing the observed MgO and FeO concentrations with those in a primary melt in the mantle, prior to fractionation,

using the expressions of Irvine (1979) and McKenzie and O'Nions (1991, 1992). The fraction of olivine removed was between 7 and 14 wt% and has no appreciable effect on the final melt fractions, which are small (Figure 5).

The melt distributions from the inversions were used to estimate the mantle potential temperature using the parameterization of hydrous mantle melting of mantle peridotite by Katz et al. (2003), which calculates the melt fraction from pressure, temperature, water content, and the modal proportion of clinopyroxene. `INVMEL` now includes this parameterization. The potential temperature was estimated by calculating the melting profile for isentropic melting, using the parameterization of Katz et al. (2003) and a water content of 238 ppm (see section 4.2), that minimizes its root mean square difference from that obtained from the inversion. Using the same parameterization and a water content of 100 ppm, the MORB source composition of McKenzie and O'Nions (1991, 1995) generates 7-km thick crust with the average composition of MORB (Gale et al., 2013) if the average potential temperature of the mantle is 1315°C (see McKenzie, 2020, for a comprehensive inversion of Gale et al.'s data).

The sensitivity of the present modeling approach to variations in input parameters was investigated by Brodie et al. (1994) and Klöcking (2018). They considered variations in the source composition and thickness and depth of the melting column and find typical uncertainties of <2% in cumulative melt fraction and 2–5 km in the depth of the top of the melting column, which amount to ±10–30°C in the estimated potential temperature. Placing the garnet-spinel transition zone at greater depth, for example, due to a greater amount of $Fe^{3+}$ or Cr in the source (Jennings & Holland, 2015), would act to increase the inferred potential temperature (Klöcking, 2018).

## 4. Results and Discussion

### 4.1. Alkali Basalts

The left column in Figure 5 shows the results of the REE inversions, grouped into four suites corresponding to the locations in Figure 1. It shows the average observed concentration (black circles ±1 SD) and the best-fitting concentration ratios calculated by the inversion (solid lines). The calculated concentrations for the NW and N groups show that the light (L-) REE concentrations are slightly underpredicted and those of the most incompatible elements (Cs, Rb, K, and Ba; third column) slightly overpredicted. These differences may result from using the primitive mantle as one of the end-members to construct a source with $\epsilon_{Nd} = 3.3$. The values of $\epsilon_{Nd}$ from basalts from oceanic islands (Stracke et al., 2003) cover a larger range than do those from the Pannonian Basin. Basalts from oceanic islands must result from melting the mantle and not from assimilation of continental crust. Those with negative $\epsilon_{Nd}$ values obviously cannot be produced from a source that is a mixture of the primitive mantle ($\epsilon_{Nd} = 0$) and the MORB source ($\epsilon_{Nd} = 10$). The compositions of such enriched regions in the mantle would require a multistage melting model to be more accurately reproduced. The application of such a model for the Pannonian basalts is considered below.

The REE inversion provides a good match to the compositions of the S and SE groups (Banat and Perşani), although the observed slope of the heavy (H-) REEs in the Perşani basalts is flatter than that calculated by single-stage melting. This behavior may result from the source having been depleted and then enriched by a metasomatic melt generated by a small amount of melting in the garnet stability field (see McKenzie & O'Nions, 1995; White & McKenzie, 1995). Here, such multistage melting comprises initial (5%) depletion of the mantle in the garnet-spinel transition zone, followed by source enrichment by a small-fraction (2%) metasomatic melt generated by minor (0.4%) melting of the MORB source at depths where garnet is stable. The dashed line in Figure 5m shows the concentration ratios resulting from such a model, which can accurately reproduce the observed pattern for Perşani. Mantle nodules brought up in Perşani show that lithospheric domains have undergone just such an evolution (Downes et al., 1992; Faccini et al., 2020; Vaselli et al., 1995).

Theoretically, such a multistage model can also improve the fits to the REEs of the NW and N groups. The dashed lines in Figures 5a and 5e show the results of such a model for these groups, whose sources were enriched by adding a small-fraction (3% and 1.5%, respectively) metasomatic melt generated by minor (0.4%) melting of the MORB source at depths where garnet is stable. It is obvious that the more complicated the model, the better the fit that can be obtained. However, none of these groups show the characteristically

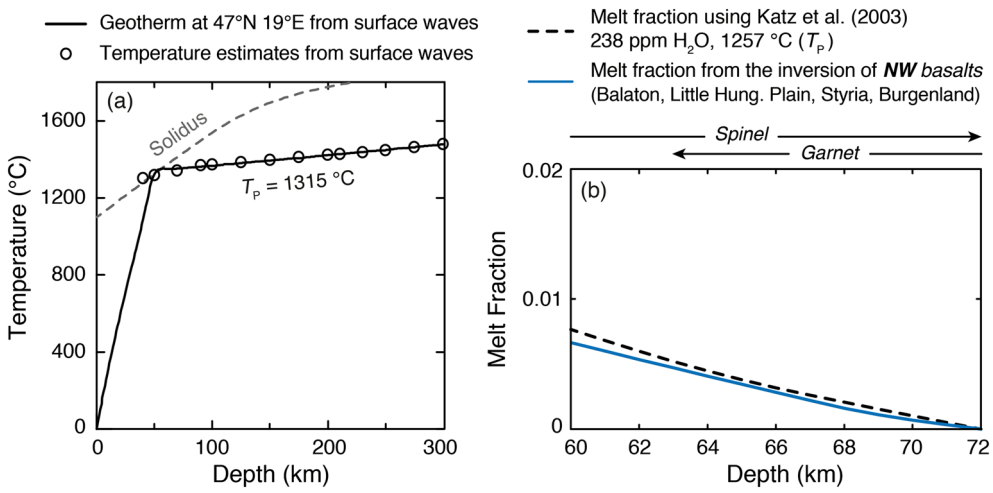


**Figure 6.** Geothermal structure of the Pannonian Basin and mantle melting parameterization. (a) Temperature estimates at the center of the Pannonian Basin (47°N, 19°E) from `CAM2016T-200` based on surface wave tomography (Priestley & McKenzie, 2013; Priestley et al., 2018). This is one of the geotherms used to determine the lithospheric thickness shown in Figures 1b (map) and 9 (profile). Shown is a mantle potential temperature ($T_P$) of 1315°C. Dry peridotite solidus after McKenzie and Bickle (1988). (b) Comparison between the melt distributions from the inversion of the NW basalts (Figure 5d; solid blue line) and that calculated from the parameterization of Katz et al. (2003) with 238 ppm $H_2O$ in the source (dashed black line). The best-fitting potential temperature is 1257°C.

flat HREE pattern as observed in Perşani, meaning that there is presently no strong argument—other than their improving the REE fit—to impose a more complex source model than that which involves single-stage melting. Importantly, both models yield nearly identical estimates of melt fractions, as well as melting depth, meaning that for the present purpose, rather than ad hoc adjustments to the source model, the simplest model is preferred. Indeed, the calculated concentrations of elements other than the REEs and Cs–Ba agree well with those observed (Figure 5, second and third column), meaning the simple mixing scenario is effective in capturing the key features.

The principal result of the modeling shown in Figure 5 is that the compositions of all the basalts from the Carpathian-Pannonian region require the mantle to have undergone less than 1% melting in the garnet-spinel transition zone. This value is slightly lower than, but probably within error of, previous estimates, that is, 2–3% (Harangi et al., 2015) or 1–4% (Seghedi et al., 2004). For Perşani, the calculated melt fraction is only slightly smaller than the 1–2% estimated from trace elements in olivine-hosted melt inclusions from Racoş, a lava flow in Perşani (Bracco Gartner et al., 2020).

### 4.2. Mantle Temperature

The presence of young basalts in small volumes that are widely distributed across the Pannonian Basin has important implications for its geothermal structure. The melt distributions calculated by the inversions can be used to estimate the potential temperature of the upper mantle from the parameterization of Katz et al. (2003). The parameterization requires an estimate of the water content of the source, here taken to be 238 ppm, calculated from estimates of the $H_2O$ content of the primitive mantle (330 ± 55 ppm) and the MORB source (100 ± 50 ppm) (Gibson & Richards, 2018, and references therein), and the average observed value of $\varepsilon_{Nd}$ (3.3) for the basalts. This estimate is corroborated by observational constraints on the water content of clinopyroxene megacrysts in the Balaton area (Kovács et al., 2020), which translates to 240 ± 90 ppm $H_2O$ in the source, using their expressions and our average melt fraction (Figure 5).

The parameterization of Katz et al. (2003) accounts for the presence of $H_2O$, but not $CO_2$, in the source. Like $H_2O$, the addition of $CO_2$ acts to lower the solidus and reduce the inferred potential temperature (e.g., Dasgupta et al., 2007, 2013). There is at present no direct measure of the $CO_2$ content of the Pannonian, or indeed most other, primary magmas, because most of the $CO_2$ is lost due to degassing during magma ascent. While there is evidence for $CO_2$-rich phases in the Pannonian lithosphere—particularly in the Balaton area—their presence is clearly linked to (earlier) subduction-related metasomatic processes, not the host basalts

(e.g., Bali, Zajacz, et al., 2008; Bali, Zanetti, et al., 2008; Créon, Delpech, et al., 2017; Créon, Rouchon, et al., 2017; Demény et al., 2004, 2010; Szabó et al., 1996). There is no evidence in the compositions of the selected basalts for a strongly carbonated source: they neither show particularly elevated CaO contents nor conspicuous trace element signatures (e.g., Sr, Ba, Zr, Hf; Veksler et al., 1998). In addition, strong effects of $CO_2$ on the melt composition, and thus inferred P-T conditions, are only expected at pressures >2 GPa, because at lower pressures, there is a major decrease in the capacity of melt to contain $CO_2$ and depress the solidus (Falloon & Green, 1989). The effect of $CO_2$, of lowering the solidus temperature, is also about three times smaller than that of $H_2O$ (Dasgupta et al., 2007). The effect of $CO_2$ is therefore likely to be minor, but nonetheless, we note that the parameterization yields an upper bound on the potential temperature.

Figure 6b compares the melt distribution from the REE inversion (Figure 5d) with that calculated from the parameterization. It shows that the two can be closely matched. The corresponding, best-fitting potential temperature to the melt distributions, of both the NW and S groups, is 1257°C. Adding 33°C, which corresponds to an isentropic gradient of 0.5°C/km, this $T_P$ corresponds to a real temperature of 1290°C at a depth of 65 km beneath the Pannonian Basin. This value exceeds temperatures estimated from the spinel peridotite nodules (mostly 900–1150°C; e.g., Dobosi et al., 2010; Embey-Isztin et al., 2001; Faccini et al., 2020; Liptai et al., 2017; Vaselli et al., 1995), which is compatible with their being derived from shallower regions in the upper mantle.

The principal question then is whether the thermal structure of the Carpathian-Pannonian upper mantle can account for the generation of melt. To map the thermal structure and lithospheric thickness in the region, we use the surface wave tomographic model of Priestley et al. (2018), which is based on the conversion of a shear wave speed ($V_{S_v}$) and anisotropy model for the upper mantle (`CAM2016Vsv`; an update of `PM_v2_2012`; Priestley & McKenzie, 2013) to a temperature model as described in Priestley and McKenzie (2013) and Priestley et al. (2018). Importantly, the parameterization $T(V_s, z)$ makes no assumptions about the rheological properties and grain size and their relationship to seismic velocity. Fitting $T(z)$ profiles with geotherms allows determination of the depth of the transition from the conducting to advecting geotherm, that is, where heat transport changes from conduction in the shallower mantle to advection in the deeper mantle. This depth corresponds to the base of the lithosphere. Both the lithospheric thickness and temperature data are available from IRIS (2018) (files `CAM2016Litho.tgz`and `CAM2016T-200.tgz`, respectively).

Figure 6a shows one of the geotherms, in the center of the Pannonian Basin (47°N, 19°E), that was used to determine the lithospheric thickness shown in Figures 1b (map) and 9 (profile). The regional geotherm shows two important features. First, it shows that the lithosphere in the center of the Basin is thin—only about 50 km. This thickness is compatible with previous estimates (e.g., Horváth, 1993; Horváth et al., 2006). Second, it shows that the temperature at the base of the lithosphere is very close to that of the dry solidus. Clearly, small volumes of melt can easily be generated near the base of the lithosphere, which indeed is just where the REE inversion shows the melting columns are located. The presence of any water in the mantle—and it is likely that there is some beneath the Basin (e.g., Aradi et al., 2017; Falus et al., 2008; Kovács et al., 2020; Lange et al., 2019; Patkó et al., 2019)—would facilitate melting at the conditions of the dry solidus.

### 4.3. Mantle Nodules

Like many alkali basalts, those from the Pannonian Basin often contain mantle nodules (e.g., Szabó et al., 2004, and references in the caption to Figure 8). Such nodules have various possible origins. They may come from the mantle with the same composition as that of the source of the basalts. Alternatively, they may come from the older, shallower part of the mantle which was stretched when the Basin formed. Whatever their origin, their composition may have been changed by infiltration of melts (such as their host basalts). A clear example of such infiltration is found in the Nógrád area, where both spinel lherzolite nodules (Liptai et al., 2017) and wehrlite nodules (of metasomatic origin; Patkó et al., 2020) were brought up by the basalts. It is of interest to compare the observed composition and mineralogy of these nodules—particularly those unaffected by extraneous metasomatic modifications—with that of the expected source of the basalts. This comparison serves to answer the question of whether some of the nodules could be fragments of basalt source rock. By reverse reasoning, finding a suitable match in the nodules also provides further validation of the calculated source used for the inversions.

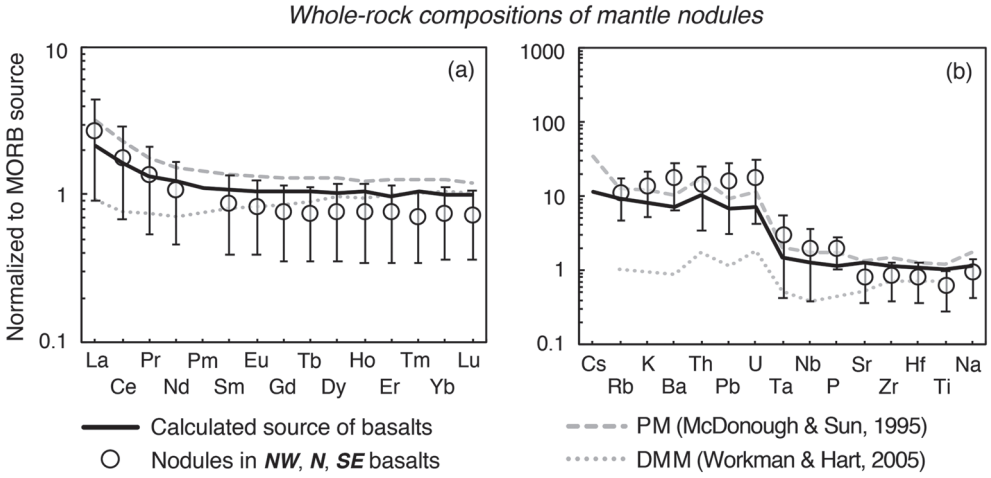


**Figure 7.** Comparison between the composition of the inferred basalt source and that of the observed mantle nodules from the Carpathian-Pannonian region. Concentrations of (a) REEs and (b) other elements in the calculated source versus the average of those observed in the whole-rock nodules. Shown for visual reference are the primitive mantle (PM) of McDonough and Sun (1995) and depleted MORB mantle (DMM) of Workman and Hart (2005) as upper and lower bounds, respectively. Average observed concentrations are weighted by the concentrations themselves (see main text). Error bars are given as ±1 SD. Concentrations are normalized to the MORB source of McKenzie and O'Nions (1991, 1995). Published nodule whole-rock trace element data (Embey-Isztin et al., 2014; Liptai et al., 2017; Ntaflos et al., 2017; Vaselli et al., 1995) are tabulated in the supporting information.

Figure 7 shows a comparison between the composition of the source used in the inversions and the average observed REE and (other) incompatible element composition of the peridotite nodules from the NW, N, and SE groups (data in supporting information). Because anomalous nodule compositions (e.g., small or otherwise unrepresentative samples) can exert disproportionate control over the average values, we identified statistical outliers in the nodule groups to obtain a more representative average composition. Outliers were identified by calculating the lower and upper quartiles $Q_1$ and $Q_3$; values outside the range $[Q_1 - 1.5(Q_3 - Q_1), Q_3 + 1.5(Q_3 - Q_1)]$ were rejected. The resulting averages are similar to the medians. Since the amount of melt that a mantle of variable composition will contribute depends on its fertility, the average composition $\bar{c}_i$ was calculated by weighting the observed concentrations $c_i^n$ by the concentrations themselves:

$$\bar{c}_i = \left[\frac{1}{N}\sum_{n=1}^{N}(c_i^n)^2\right]^{1/2} \tag{2}$$

where $N$ is the number of samples. The composition of the nodules is clearly variable; the error bars on the concentrations in Figure 7 correspond to 1 SD. Nonetheless, the figure shows that the average observed REE and incompatible element composition of the Pannonian peridotite nodules is similar to that of the source used in the inversions. This consistency suggests that these nodule suites may in fact be fragments of source rock, which were entrained by the magmas they generated. The REE inversions, however, require the melt to be generated within the garnet-spinel transition zone, and none of the nodules contain garnet. Therefore, as might be expected, they must come from depths that are shallower than the source regions of the basalts.

More insight is provided by comparing the mineralogy and clinopyroxene composition of the nodules and those of the calculated source. The calculated composition of clinopyroxene in the source depends on the mineral mode, which, because the source region spans the garnet-spinel transition zone, in turn depends on depth. For direct comparison with the nodules, it is therefore most informative to consider the source characteristics at depths where spinel, and not garnet, is stable. Figure 8a compares the mineral mode of the source, calculated for a spinel peridotite whose bulk composition is the same as that of the source used in the inversions ($Ol_{0.58}Opx_{0.27}Cpx_{0.12}Sp_{0.03}$), to the average of that observed in the nodules. In addition, Figure 8b compares the average composition of "LREE-depleted" clinopyroxenes in nodules from the NW (Dobosi et al., 2010; Embey-Isztin et al., 2014), N (Liptai et al., 2017), and SE (Faccini et al., 2020)—which are thought to represent the unmetasomatized, or "precursor," mantle beneath their respective regions—

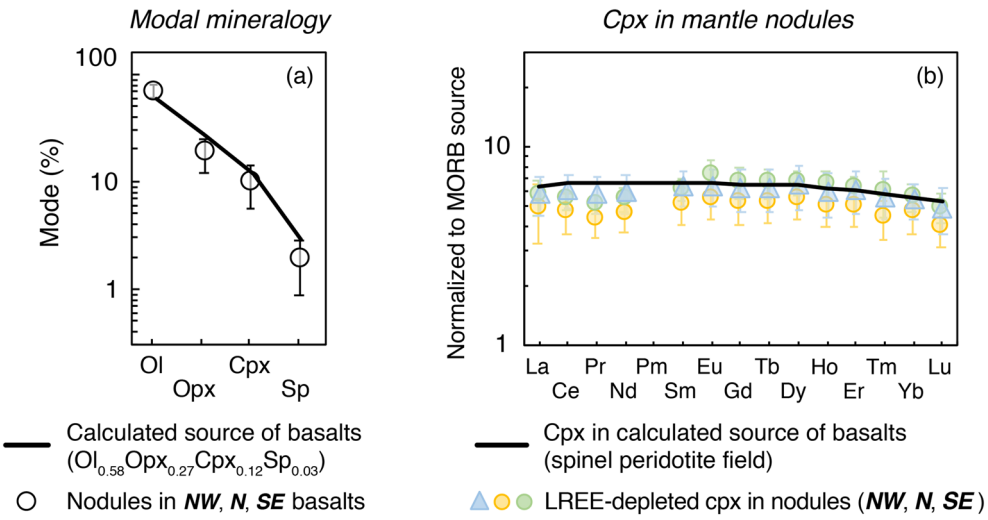


**Figure 8.** Comparison between the inferred basalt source and the observed mantle nodules from the Carpathian-Pannonian region. (a) Modal mineralogy of the calculated source versus the average of that observed in nodules from the NW, N, and SE groups. Ol = olivine; Opx = orthopyroxene; Cpx = clinopyroxene; Sp = spinel. Published nodule data (Aradi et al., 2017; Downes et al., 1992; Embey-Isztin et al., 1989, 1990, 2014; Faccini et al., 2020; Liptai et al., 2017; Ntaflos et al., 2017; Szabó & Taylor, 1994; Szabó et al., 1995; Vaselli et al., 1995, 1996) are tabulated in the supporting information. Note that statistical outliers were identified according to the criteria described in the main text; samples were excluded if outlying modes were identified. (b) REE distributions in clinopyroxene in the basalt source, calculated for a spinel peridotite whose bulk composition is the same as that of the source used in the inversions, versus those observed in "LREE-depleted" clinopyroxene in the nodules (data in supporting information; Dobosi et al., 2010; Embey-Isztin et al., 2014; Faccini et al., 2020; Liptai et al., 2017). Average observed concentrations are weighted by the concentrations themselves (see main text). Error bars are given as ±1 SD. Concentrations are normalized to the MORB source of McKenzie and O'Nions (1991).

with that calculated for clinopyroxene in the source, also at depths where spinel is stable. Both the expected mineral mode and the clinopyroxene composition of the basalt source closely resemble that of the nodule suites and are consistent with their representing the basalt source rock.

In summary, there is strong consistency between the calculated basalt source and the observational data (bulk-rock trace elements, mineralogy, and clinopyroxene REEs) from various suites of mantle "xenoliths" that were brought up by these magmas throughout the region. It is probably better to refer to all such inclusions as nodules, rather than xenoliths, because, like those discussed here, they may be pieces of the source rock, not foreign inclusions. The principal difference between the basalt source and the mantle nodules concerns the depth at which they equilibrated: the garnet-free nodules must originate from depths shallower than the source regions of the basalts.

### 4.4. Melt Generation and Intraplate Volcanism

The REE inversions show that fractional melting of a homogeneous source can reproduce the elemental compositions of the erupted basalts in the Carpathian-Pannonian region. The composition of this source, here termed PUMA (supporting information), is similar to that of some of the mantle material brought up as nodules throughout the region. These results do not imply that the melt source is homogeneous; it rather suggests that any small-scale lithological or compositional heterogeneities present in the source region were homogenized as the melts rose to the surface. It is probable that the source regions contain small-scale inhomogeneities like those beneath other basaltic volcanoes.

The inversions show that the young intraplate basalts in the Carpathian-Pannonian region are sourced from the garnet-spinel transition zone, at depths of about 63–72 km. Figure 9 shows a section across the Pannonian Basin along the profile trace shown in Figure 1b and illustrates the Basin's geophysical architecture derived from the surface wave tomography of Priestley and McKenzie (2013) and Priestley et al. (2018) (see Figure 6a). The base of the lithosphere is at a temperature of about 1300°C and melt is generated within the garnet-spinel transition zone, where the geotherm reaches the solidus. Figure 9 shows that all the

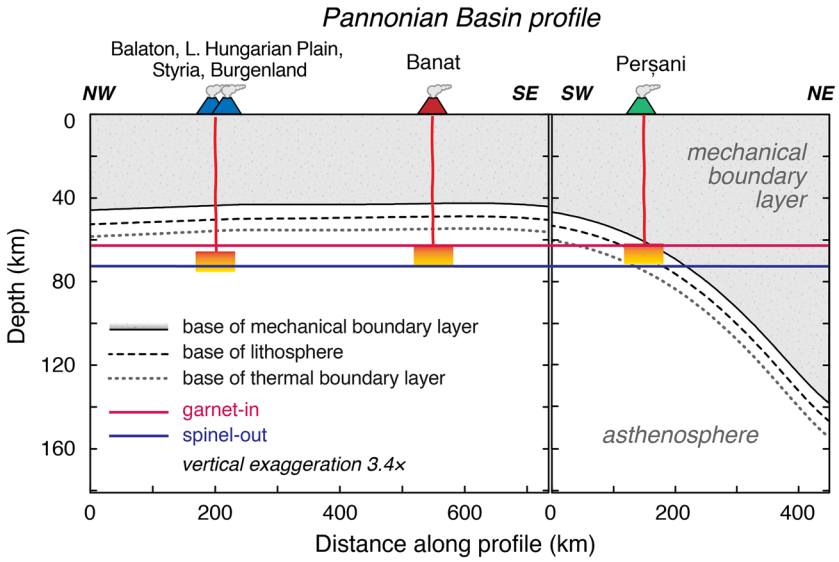


**Figure 9.** Schematic profile through the Carpathian-Pannonian region that illustrates the melting columns for the Late Miocene–Quaternary intraplate basalts. Profile trace is shown in Figure 1b. Vertical exaggeration is 3.4×. Base of the lithosphere and thermal and mechanical boundary layers are derived from surface wave tomography (see Figure 6a; Priestley & McKenzie, 2013; Priestley et al., 2018). Depths of the melting columns are derived from the rare earth element inversions (see Figure 5).

magmas beneath the Basin are probably sourced from the asthenosphere, close to the base of the thermal boundary layer.

The thin lithosphere is a result of extension, which occurred when the subduction zone beneath the Carpathian arc rolled back (Balázs et al., 2016; Horváth et al., 2006; Royden, 1988; Ustaszewski et al., 2008). The same process is now taking place in the Aegean further south (e.g., Jolivet & Brun, 2010). Subduction stopped in the northeast when it reached the thick lithosphere of the Russian Platform (see Figure 1b). Because the extension rate was slow, mantle upwelling was not sufficiently fast to generate large volumes of melt. Any small volumes that erupted were buried beneath sediments in those parts of the Basin that were rapidly subsiding (e.g., Zelenka et al., 2004). Heat loss to the surface allowed the upwelling mantle to cool below its solidus and to become part of the mechanical boundary layer. Some of this material has then been brought to the surface as spinel peridotite nodules in the magmas. Yet when volcanism appears to flare up, in the Late Miocene, the extension in the Pannonian Basin had effectively ceased. What causes these melts to form and rise up from beneath the plate's interior?

The gravity anomalies and topography of the Basin (Figure 2) show no systematic pattern of swells and/or troughs at wavelengths between 100 km and that of the Basin, ~500 km. These features signify that there is no large, hot structure present immediately beneath the plate's interior. Just as the small melt fractions imply, and other studies have construed (e.g., Embey-Isztin, Downes, et al., 1993; Huismans et al., 2001), the nature of the volcanism is clearly not compatible with an extensive thermal plume. Instead, the lithospheric thickness (Figure 1b) and geotherm (Figure 6a) show that melting occurs because the base of the lithosphere is close to or at the solidus temperature over a large part of the Basin. This observation is corroborated by the calculated conditions of mantle-melt equilibration based on the major element content of the basalts (Harangi et al., 2015), which similarly suggest that the sublithospheric upper mantle is at a temperature close to the peridotite solidus.

Only the Perşani volcanics appear to be underlain by slightly thicker lithosphere than those in the Pannonian Basin. However, unlike the vertical resolution (30–40 km), the horizontal resolution of the surface wave tomography is 200–300 km (Priestley & McKenzie, 2013) and is therefore not sufficient to resolve the vertical slab beneath Vrancea (as imaged by e.g., Martin & Wenzel, 2006). Because intraplate volcanism in Perşani developed only about 100 km northwest of this region, contemporaneously with the last episodes of calc-alkaline volcanism in the southern East Carpathians (Seghedi et al., 2016), it should probably be

considered as being separate from the volcanism in the Pannonian Basin. Focal mechanisms of the subcrustal earthquakes beneath Vrancea hint at the past subduction of oceanic lithosphere that is presently undergoing down-dip extension (McKenzie et al., 2019). Crustal fault systems in the Perşani Mountains (Seghedi et al., 2016) show that extensional tectonics were instrumental in the development of volcanism. We concur with Seghedi et al. (2011) that steepening and rollback of the Vrancea slab is most likely to have driven the lithospheric stretching that gave rise to small-degree melting beneath Perşani.

By contrast, intraplate volcanism in the Pannonian Basin during the Quaternary is clearly not the result of ongoing extension. Though the amount of melting is small, the time difference between the extension and volcanism cannot be due to the slow movement of melt. There is strong evidence, both theoretical and observational, that small melt fractions ($\leq$0.5%, down to 0.2%) separate rapidly (on a time scale of ~1 ka) from their residues, with no appreciable volume remaining in the source region (e.g., Eksinchol et al., 2019; Jull & McKenzie, 1996; Kokfelt et al., 2003; Liang & Peng, 2010; McKenzie, 1985; Slater et al., 2001). Furthermore, unless, for example, water or carbon dioxide is introduced into the mantle, the solidus temperature is a monotonically increasing function of depth. Therefore, it appears that there must be some upwelling to account for the volcanism. Since the lithosphere is cooling and its thickness is increasing after the stretching event, this upwelling and melting is more likely to occur in the asthenosphere than in the lithosphere. This is consistent with our results (Figure 9), which show that the melts seem to originate from the asthenosphere immediately below the lithosphere. Such upwelling can produce melts because the lithosphere is thin and the upwelling material is hotter than that which surrounds it. However, because the volume of melt is so small (i.e., <1% melting, amounting to just a few cubic kilometers of lava throughout the Basin), the upwelling clearly moves mantle material upwards just enough for it to cross its solidus.

The geometry of such upwelling is not well constrained by the surface observations (Figure 2). The viscosity of the asthenosphere near the top of the mantle is probably about $10^{19}$ Pa·s. Such a low viscosity means that the gravity anomalies and dynamic topography resulting from the hot upwelling will be small. It is then difficult to distinguish the surface expression of such upwelling from gravity anomalies and topography generated by the variations in crustal thickness that resulted from the earlier tectonic deformation. The volume of the volcanism is small, and probably overlies centers of upwelling, but it is not yet possible to confirm the existence or the geometry of the upwelling using other types of observations. Because the topography and gravity anomalies are dominated by the recent tectonics, the presence of young basalts widely distributed across the Basin appears at present to be the only clearly discernible signal of vertical convective motion beneath the area.

It is important to emphasize that the combined geophysical and geochemical constraints described here do not necessitate, and are not compatible with, a major thermal plume as a causal mechanism for melt generation. Instead, the results are more compatible with previous studies that surmised a link between lithospheric thinning and subsequent decompression-induced mantle melting (e.g., Embey-Isztin, Downes, et al., 1993; Seghedi et al., 2004; Wilson & Downes, 1991). Clearly, only a small amount of upwelling is needed to form minor volumes (up to a few cubic kilometers) of basaltic melt immediately below the lithosphere when its base is close to the solidus temperature. Though the thinned lithosphere of the Carpathian-Pannonian region is the result of stretching, ongoing extension is not a prerequisite for the formation of intraplate volcanism. What appears to be required is a relatively thin lithosphere, below which thermal buoyancy is likely to drive upwelling and hence melt production.

## 5. Conclusions

To place constraints on the generation of melt and its source region beneath young (12–0.1 Ma) Carpathian-Pannonian intraplate volcanoes, we modeled the geochemistry of the erupted basalts and mantle nodules and integrated the results with evidence from surface wave tomography, gravity anomalies, and topography.

1. The REE inversion and forward calculation of elemental concentrations are found to provide close fits to the observed compositions of the basalts. The inversion shows that their composition requires the mantle to have undergone less than 1% melting in the garnet-spinel transition zone, corresponding to a depth range of about 63 to 72 km, that is, in the shallow upper mantle just below the base of the lithosphere.

2. Using the melt distributions from the inversions and a parameterization of mantle melting, we obtain a mantle potential temperature of ~1257°C. It corresponds to a real temperature of 1290°C at a depth of 65 km beneath the Pannonian Basin and is compatible with the observed volume of volcanic rock and the small melt fractions involved.
3. The composition, mineral modes, and clinopyroxene geochemistry of some of the mantle nodules brought up by the basalts throughout the region closely resemble those calculated for the basalt source. The principal difference is that the basalt source equilibrated at greater depths.
4. The lithospheric thickness and geotherm show that melting occurs because the base of the lithosphere, at ~50-km depth, is close to or at the solidus temperature over a large part of the Basin. The volcanism appears to originate from upwelling in the asthenosphere just below the thinned lithosphere, which moves mantle material upwards just enough for it to cross its solidus and produce small volumes (up to a few cubic kilometers) of melt.
5. Because the topography and gravity anomalies of the Basin are dominated by earlier tectonic deformation, the post-extensional volcanism seems at present to be the only discernible signal that resolves the details of vertical convective motion beneath the region.

## Appendix A: Mineral-Melt Partition Coefficients

Table S1 lists all the mineral-melt partition coefficients for the REEs (used in the inversion) and elements other than the REEs (used in the forward modeling). Partition coefficients are taken from Beattie (1993), Johnson (1998), Mallmann and O'Neill (2009), and McKenzie and O'Nions (1991, 1995), except for the REEs in clinopyroxene and garnet.

The lattice-strain model of Blundy and Wood (1994) and Wood and Blundy (1997) based on Brice (1975) was used to obtain a consistent set of partition coefficients for REEs in clinopyroxene and garnet and obtain values for those REEs for which no (reliable) measurements are available. Their expression for the partition coefficient for element $i$ ($D_i$) with ionic radius $r_i$ between a particular mineral and melt is

$$D_i \equiv \frac{c_s}{c_l} = D_0 \exp\left[\frac{-4\pi E N_A}{RT_k}\left[\frac{r_0}{2}(r_i - r_o)^2 + \frac{1}{3}(r_i - r_0)^3\right]\right] \quad \text{(A1)}$$

where $c_s$ and $c_l$ are the elemental concentrations in the solid and liquid, respectively; $N_A$ is Avogadro's number; $R$ is the gas constant; and $T_k$ the absolute temperature. The radius of the crystallographic site ($r_o$), the Young's modulus ($E$) of that site, and the strain-free partition coefficient ($D_0$) are constants that depend on the mineral and the valency of the substituting element. These constants were calculated for clinopyroxene and garnet by fitting Brice's expression to the $D$ values of McKenzie and O'Nions (1991)

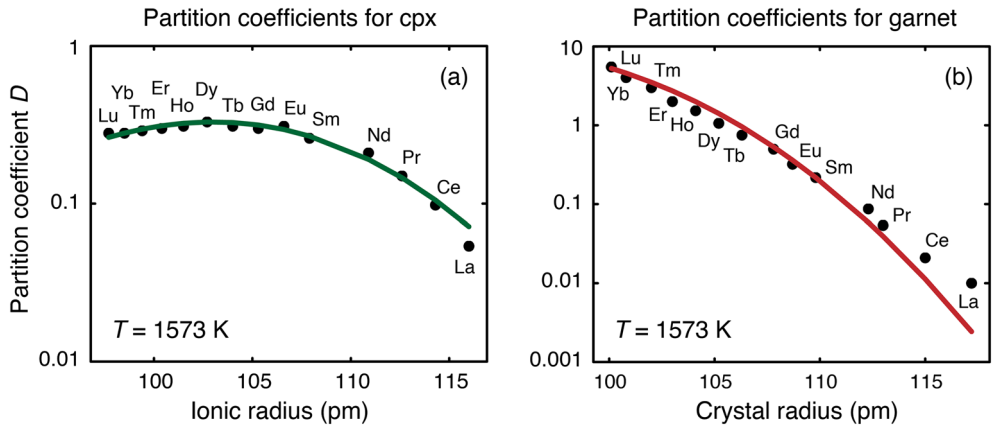


**Figure A1.** Partition coefficients $D$ for trivalent rare earth elements in (a) clinopyroxene (cpx) and (b) pyrope garnet as a function of ionic and crystal radius (in pm), respectively. Constants $D_0$, $r_0$, and $E$ for clinopyroxene and garnet were determined by fitting the expression of Blundy and Wood (1994) and Brice (1975) (Equation A1) to the $D$ values of McKenzie and O'Nions (1991) (black dots) using $T = 1573$ K. Solid lines denote the $D$ values that were subsequently calculated using Equation A1 and the respective constants.

using $T = 1573$ K (Figure A1). The resultant values are 103.0 and 93 pm ($r_0$), 279.5 and 450 GPa ($E$), and 0.330 and 10 ($D_0$), respectively. The $D$ values for trivalent REEs and Y were calculated assuming substitution in the clinopyroxene M2-site with eightfold coordination and garnet Y-site with sixfold coordination, using the effective ionic and crystal radii of Shannon (1976), respectively.

## Appendix B: Melt Source Compositions

Table S2 lists the compositions of the MORB source and primitive mantle of McKenzie and O'Nions (1991, 1995) and that of the calculated source. Concentrations of $H_2O$ in the MORB source and primitive mantle are from Gibson and Richards (2018) and references therein. The calculated source, termed Pannonian Upper MAntle (PUMA), was calculated by combining the MORB source and primitive mantle in appropriate fractions to generate a source with $\epsilon_{Nd} = 3.3$ (the average observed value for the Pannonian basalts).

## Appendix C: Basalt and Nodule Data Sources

Tables S3 to S6 list the geochemical data on the alkali basalts and mantle nodules from the Carpathian-Pannonian region that were used for the modeling and comparisons shown in the main text.

## Data Availability Statement

Data sets for this research are included in the supporting information file of this paper. In-text citation references are as follows: basalt compositions (Ali & Ntaflos, 2011; Ali et al., 2013; Dobosi et al., 1995; Dobosi & Jenner, 1999; Downes et al., 1995; Ducea et al., 2020; Embey-Isztin, Dobosi, et al., 1993; Embey-Isztin, Downes, et al., 1993; Harangi et al., 1994, 2013, 2015; Harangi, Vaselli, et al., 1995; Ivan & Hovorka, 1993; Jankovics et al., 2015, 2019; Rosenbaum et al., 1997; Tschegg et al., 2010); nodule compositions and mineralogy (Aradi et al., 2017; Dobosi et al., 2010; Downes et al., 1992; Embey-Isztin et al., 1989, 1990; Embey-Isztin et al., 2014; Faccini et al., 2020; Liptai et al., 2017; Ntaflos et al., 2017; Szabó & Taylor, 1994; Szabó et al., 1995; Vaselli et al., 1995, 1996); mineral-melt partition coefficients (Beattie, 1993; Johnson, 1998; Mallmann & O'Neill, 2009; McKenzie & O'Nions, 1991, 1995); melt sources (Gibson & Richards, 2018; McKenzie & O'Nions, 1991, 1995). Software for this research, that is, the `INVMEL` scheme formulated by McKenzie and O'Nions (1991, 1995), has since its conception been expanded to include the mantle melting parameterization of Katz et al. (2003) and the partition coefficient parameterization of Blundy and Wood (1994) and is contained in these in-text citation references. Global topography 1-min grid (Smith & Sandwell, 1997) is available online (https://topex.ucsd.edu/marine_topo/; version 19.1). `EIGEN-6C` global combined gravity field model (Shako et al., 2014) is also available online (https://doi.org/10.5880/icgem.2015.1) (Förste et al., 2014). Lithospheric thickness and temperature data from surface wave tomography (Priestley & McKenzie, 2013; Priestley et al., 2018) are available from IRIS (2018) (https://doi.org/10.17611/DP/EMCCAM2016; files `CAM2016Litho.tgz` and `CAM2016T-200.tgz`, respectively).

**Acknowledgments**

We thank Bill White, Godfrey Fitton, and an anonymous reviewer for their constructive reviews, and Janne Blichert-Toft for editorial handling. We also thank two anonymous reviewers whose perceptive comments helped to improve an earlier version of this paper. A. J. J. B. G. would like to thank Ioan Seghedi for his help and suggestions. During the writing of this paper, A. J. J. B. G. received funding from the European Research Council (ERC) under the European Union's Horizon 2020 research and innovation program (grant agreement 759563). A. J. J. B. G. conceived the project and wrote the paper. D. M. carried out the modeling.

## References

Ali, S., & Ntaflos, T. (2011). Alkali basalts from Burgenland, Austria: Petrological constraints on the origin of the westernmost magmatism in the Carpathian-Pannonian region. *Lithos*, *121*(1–4), 176–188. https://doi.org/10.1016/J.LITHOS.2010.11.001

Ali, S., Ntaflos, T., & Upton, B. G. (2013). Petrogenesis and mantle source characteristics of Quaternary alkaline mafic lavas in the western Carpathian-Pannonian region, Styria, Austria. *Chemical Geology*, *337–338*, 99–113. https://doi.org/10.1016/J.CHEMGEO.2012.12.001

Aradi, L. E., Hidas, K., Kovács, I. J., Tommasi, A., Klébesz, R., Garrido, C. J., & Szabó, C. (2017). Fluid-enhanced annealing in the subcontinental lithospheric mantle beneath the westernmost margin of the Carpathian-Pannonian extensional basin system. *Tectonics*, *36*, 2987–3011. https://doi.org/10.1002/2017TC004702

Balázs, A., Burov, E., Matenco, L., Vogt, K., Francois, T., & Cloetingh, S. (2017). Symmetry during the syn- and post-rift evolution of extensional back-arc basins: The role of inherited orogenic structures. *Earth and Planetary Science Letters*, *462*, 86–98. https://doi.org/10.1016/J.EPSL.2017.01.015

Balázs, A., Matenco, L., Magyar, I., Horváth, F., & Cloetingh, S. (2016). The link between tectonics and sedimentation in back-arc basins: New genetic constraints from the analysis of the Pannonian Basin. *Tectonics*, *35*, 1526–1559. https://doi.org/10.1002/2015TC004109

Bali, E., Zajacz, Z., Kovacs, I., Szabó, C., Halter, W., Vaselli, O., et al. (2008). A quartz-bearing orthopyroxene-rich websterite xenolith from the Pannonian Basin, Western Hungary: Evidence for release of quartz-saturated melts from a subducted slab. *Journal of Petrology*, *49*(3), 421–439. https://doi.org/10.1093/petrology/egm086

Bali, E., Zanetti, A., Szabó, C., Peate, D. W., & Waight, T. E. (2008). A micro-scale investigation of melt production and extraction in the upper mantle based on silicate melt pockets in ultramafic xenoliths from the Bakony-Balaton Highland volcanic field (Western Hungary). *Contributions to Mineralogy and Petrology*, *155*(2), 165–179. https://doi.org/10.1007/s00410-007-0234-4

Ball, P. W., White, N. J., Masoud, A., Nixon, S., Hoggard, M. J., Maclennan, J., et al. (2019). Quantifying asthenospheric and lithospheric controls on mafic magmatism across North Africa. *Geochemistry, Geophysics, Geosystems*, *20*, 3520–3555. https://doi.org/10.1029/2019GC008303

Ballmer, M. D., van Hunen, J., Ito, G., Tackley, P. J., & Bianco, T. A. (2007). Non-hotspot volcano chains originating from small-scale sublithospheric convection. *Geophysical Research Letters*, *34*, L23310. https://doi.org/10.1029/2007GL031636

Beattie, P. (1993). Uranium-thorium disequilibria and partitioning on melting of garnet peridotite. *Nature*, *363*(6424), 63–65. https://doi.org/10.1038/363063a0

Blundy, J., & Wood, B. (1994). Prediction of crystal-melt partition coefficients from elastic moduli. *Nature*, *372*(6505), 452–454. https://doi.org/10.1038/372452a0

Bracco Gartner, A. J. J., Seghedi, I., Nikogosian, I. K., & Mason, P. R. D. (2020). Asthenosphere-induced melting of diverse source regions for East Carpathian post-collisional volcanism. *Contributions to Mineralogy and Petrology*, *175*(6), 54. https://doi.org/10.1007/s00410-020-01690-4

Brice, J. C. (1975). Some thermodynamic aspects of the growth of strained crystals. *Journal of Crystal Growth*, *28*(2), 249–253. https://doi.org/10.1016/0022-0248(75)90241-9

Brodie, J., Latin, D., & White, N. (1994). Rare earth element inversion for melt distribution: Sensitivity and application. *Journal of Petrology*, *35*(4), 1155–1174. https://doi.org/10.1093/petrology/35.4.1155

Brown, E. L., & Lesher, C. E. (2016). REEBOX PRO: A forward model simulating melting of thermally and lithologically variable upwelling mantle. *Geochemistry, Geophysics, Geosystems*, *17*, 3929–3968. https://doi.org/10.1002/2016GC006579

Conrad, C. P., Wu, B., Smith, E. I., Bianco, T. A., & Tibbetts, A. (2010). Shear-driven upwelling induced by lateral viscosity variations and asthenospheric shear: A mechanism for intraplate volcanism. *Physics of the Earth and Planetary Interiors*, *178*(3–4), 162–175. https://doi.org/10.1016/J.PEPI.2009.10.001

Créon, L., Delpech, G., Rouchon, V., & Guyot, F. (2017). Slab-derived metasomatism in the Carpathian-Pannonian mantle revealed by investigations of mantle xenoliths from the Bakony-Balaton Highland volcanic field. *Lithos*, *286–287*, 534–552. https://doi.org/10.1016/j.lithos.2017.06.004

Créon, L., Rouchon, V., Youssef, S., Rosenberg, E., Delpech, G., Szabó, C., et al. (2017). Highly $CO_2$-supersaturated melts in the Pannonian lithospheric mantle—A transient carbon reservoir? *Lithos*, *286–287*, 519–533. https://doi.org/10.1016/j.lithos.2016.12.009

Dasgupta, R., Hirschmann, M. M., & Smith, N. D. (2007). Water follows carbon: $CO_2$ incites deep silicate melting and dehydration beneath mid-ocean ridges. *Geology*, *35*(2), 135. https://doi.org/10.1130/G22856A.1

Dasgupta, R., Mallik, A., Tsuno, K., Withers, A. C., Hirth, G., & Hirschmann, M. M. (2013). Carbon-dioxide-rich silicate melt in the Earth's upper mantle. *Nature*, *493*(7431), 211–215. https://doi.org/10.1038/nature11731

Demény, A., Dallai, L., Frezzotti, M.-L., Vennemann, T. W., Embey-Isztin, A., Dobosi, G., & Nagy, G. (2010). Origin of $CO_2$ and carbonate veins in mantle-derived xenoliths in the Pannonian Basin. *Lithos*, *117*(1–4), 172–182. https://doi.org/10.1016/j.lithos.2010.02.013

Demény, A., Vennemann, T. W., Hegner, E., Nagy, G., Milton, J. A., Embey-Isztin, A., et al. (2004). Trace element and C-O-Sr-Nd isotope evidence for subduction-related arbonate-silicate melts in mantle xenoliths (Pannonian Basin, Hungary). *Lithos*, *75*(1–2), 89–113. https://doi.org/10.1016/j.lithos.2003.12.016

Dobosi, G., Fodor, R. V., & Goldberg, S. A. (1995). Late-Cenozoic alkalic basalt magmatism in Northern Hungary and Slovakia: Petrology, source compositions and relationship to tectonics. *Acta Vulcanologica*, *7*, 199–207.

Dobosi, G., & Jenner, G. A. (1999). Petrologic implications of trace element variation in clinopyroxene megacrysts from the Nógrád volcanic province, north Hungary: A study by laser ablation microprobe-inductively coupled plasma-mass spectrometry. *Lithos*, *46*(4), 731–749. https://doi.org/10.1016/S0024-4937(98)00093-0

Dobosi, G., Jenner, G. A., Embey-Isztin, A., & Downes, H. (2010). Cryptic metasomatism in clino- and orthopyroxene in the upper mantle beneath the Pannonian region. *Geological Society, London, Special Publications*, *337*(1), 177–194. https://doi.org/10.1144/SP337.9

Dombrádi, E., Sokoutis, D., Bada, G., Cloetingh, S., & Horváth, F. (2010). Modelling recent deformation of the Pannonian lithosphere: Lithospheric folding and tectonic topography. *Tectonophysics*, *484*(1–4), 103–118. https://doi.org/10.1016/J.TECTO.2009.09.014

Downes, H., Embey-Isztin, A., & Thirlwall, M. F. (1992). Petrology and geochemistry of spinel peridotite xenoliths from the western Pannonian Basin (Hungary): Evidence for an association between enrichment and texture in the upper mantle. *Contributions to Mineralogy and Petrology*, *109*(3), 340–354. https://doi.org/10.1007/BF00283323

Downes, H., Seghedi, I., Szakács, A., Dobosi, G., James, D. E., Vaselli, O., et al. (1995). Petrology and geochemistry of late Tertiary/Quaternary mafic alkaline volcanism in Romania. *Lithos*, *35*, 65–81. https://doi.org/10.1016/0024-4937(95)91152-Y

Ducea, M. N., Barla, A., Stoica, A. M., Panaiotu, C., & Petrescu, L. (2020). Temporal-geochemical evolution of the Persani volcanic field, eastern Transylvanian Basin (Romania): Implications for slab rollback beneath the SE Carpathians. *Tectonics*, *39*, e2019TC005802. https://doi.org/10.1029/2019TC005802

Eksinchol, I., Rudge, J. F., & Maclennan, J. (2019). Rate of melt ascent beneath Iceland from the magmatic response to deglaciation. *Geochemistry, Geophysics, Geosystems*, *20*, 2585–2605. https://doi.org/10.1029/2019GC008222

Embey-Isztin, A., Dobosi, G., Altherr, R., & Meyer, H.-P. (2001). Thermal evolution of the lithosphere beneath the western Pannonian Basin: Evidence from deep-seated xenoliths. *Tectonophysics*, *331*(3), 285–306. https://doi.org/10.1016/S0040-1951(00)00287-0

Embey-Isztin, A., Dobosi, G., Bodinier, J.-L., Bosch, D., Jenner, G. A., Pourtales, S., & Bruguier, O. (2014). Origin and significance of poikilitic and mosaic peridotite xenoliths in the western Pannonian Basin: Geochemical and petrological evidences. *Contributions to Mineralogy and Petrology*, *168*(3), 1054. https://doi.org/10.1007/s00410-014-1054-y

Embey-Isztin, A., Dobosi, G., James, D., Downes, H., Poultidis, C., & Scharbert, H. G. (1993). A compilation of new major, trace element and isotope geochemical analyses of the young alkali basalts from the Pannonian Basin. *Fragmenta Mineralogica et Palaeontologica*, *16*, 5–26.

Embey-Isztin, A., Downes, H., James, D. E., Upton, B. G. J., Dobosi, G., Ingram, G. A., et al. (1993). The petrogenesis of Pliocene alkaline volcanic rocks from the Pannonian Basin, eastern Central Europe. *Journal of Petrology*, *34*(2), 317–343.

Embey-Isztin, A., Scharbert, H. G., Dietrich, H., & Poultidis, H. (1989). Petrology and geochemistry of peridotite xenoliths in alkali basalts from the Transdanubian volcanic region, West Hungary. *Journal of Petrology*, *30*(1), 79–105. https://doi.org/10.1093/petrology/30.1.79

Embey-Isztin, A., Scharbert, H. G., Dietrich, H., & Poultidis, H. (1990). Mafic granulites and clinopyroxenite xenoliths from the Transdanubian volcanic region (Hungary): Implications for the deep structure of the Pannonian Basin. *Mineralogical Magazine*, *54*(376), 463–483. https://doi.org/10.1180/minmag.1990.054.376.12

Faccini, B., Rizzo, A. L., Bonadiman, C., Ntaflos, T., Seghedi, I., Grégoire, M., et al. (2020). Subduction-related melt refertilisation and alkaline metasomatism in the Eastern Transylvanian Basin lithospheric mantle: Evidence from mineral chemistry and noble gases in fluid inclusions. *Lithos*, *364–365*, 105516. https://doi.org/10.1016/j.lithos.2020.105516

Falloon, T. J., & Green, D. H. (1989). The solidus of carbonated, fertile peridotite. *Earth and Planetary Science Letters*, *94*(3–4), 364–370. https://doi.org/10.1016/0012-821X(89)90153-2

Falus, G., Tommasi, A., Ingrin, J., & Szabó, C. (2008). Deformation and seismic anisotropy of the lithospheric mantle in the southeastern Carpathians inferred from the study of mantle xenoliths. *Earth and Planetary Science Letters*, *272*(1–2), 50–64. https://doi.org/10.1016/J.EPSL.2008.04.035

Förste, C., Bruinsma, S. L., Abrikosov, O., Lemoine, J.-M., Marty, J. C., Flechtner, F., et al. (2014). EIGEN-6C4 The latest combined global gravity field model including GOCE data up to degree and order 2190 of GFZ Potsdam and GRGS Toulouse. GFZ Data Services. https://doi.org/10.5880/icgem.2015.1

Foulger, G. R., & Natland, J. H. (2003). Is "hotspot" volcanism a consequence of plate tectonics? *Science*, *300*(5621), 921–922. https://doi.org/10.1126/science.1083376

Gale, A., Dalton, C. A., Langmuir, C. H., Su, Y., & Schilling, J.-G. (2013). The mean composition of ocean ridge basalts. *Geochemistry, Geophysics, Geosystems*, *14*, 489–518. https://doi.org/10.1029/2012GC004334

Ghiorso, M. S., Hirschmann, M. M., Reiners, P. W., & Kress, V. C. (2002). The pMELTS: A revision of MELTS for improved calculation of phase relations and major element partitioning related to partial melting of the mantle to 3 GPa. *Geochemistry, Geophysics, Geosystems*, *3*(5), 1–35. https://doi.org/10.1029/2001GC000217

Gibson, S. A., & Richards, M. A. (2018). Delivery of deep-sourced, volatile-rich plume material to the global ridge system. *Earth and Planetary Science Letters*, *499*, 205–218. https://doi.org/10.1016/J.EPSL.2018.07.028

Harangi, S., Jankovics, M. E., Sági, T., Kiss, B., Lukács, R., & Soós, I. (2015). Origin and geodynamic relationships of the Late Miocene to Quaternary alkaline basalt volcanism in the Pannonian Basin, eastern-central Europe. *International Journal of Earth Sciences*, *104*(8), 2007–2032. https://doi.org/10.1007/s00531-014-1105-7

Harangi, S., Sági, T., Seghedi, I., & Ntaflos, T. (2013). Origin of basaltic magmas of Perşani volcanic field, Romania: A combined whole rock and mineral scale investigation. *Lithos*, *180–181*, 43–57. https://doi.org/10.1016/j.lithos.2013.08.02

Harangi, S., Vaselli, O., Kovacs, R., Tonarini, S., Coradossi, N., & Ferraro, D. (1994). Volcanological and magmatological studies on the Neogene basaltic volcanoes of the southern Little Hungarian Plain, Pannonian Basin (western Hungary). *Mineralogica et Petrographica Acta*, *37*, 183–197.

Harangi, S., Vaselli, O., Tonarini, S., Szabó, C., Harangi, R., & Coradossi, N. (1995). Petrogenesis of Neogene extension-related alkaline volcanic rocks of the Little Hungarian Plain Volcanic Field (Western Hungary). *Acta Vulcanologica*, *7*(2), 173–187.

Harangi, S., Wilson, M., & Tonarini, S. (1995). Petrogenesis of Neogene potassic volcanic rocks in the Pannonian Basin. *Acta Vulcanologica*, *7*(2), 125–134.

Horváth, F. (1993). Towards a mechanical model for the formation of the Pannonian Basin. *Tectonophysics*, *226*(1–4), 333–357. https://doi.org/10.1016/0040-1951(93)90126-5

Horváth, F., Bada, G., Szafián, P., Tari, G., Ádám, A., & Cloetingh, S. (2006). Formation and deformation of the Pannonian Basin: Constraints from observational data. *Geological Society, London, Memoirs*, *32*(1), 191–206. https://doi.org/10.1144/GSL.MEM.2006.032.01.11

Horváth, F., Musitz, B., Balázs, A., Végh, A., Uhrin, A., Nádor, A., et al. (2015). Evolution of the Pannonian Basin and its geothermal resources. *Geothermics*, *53*, 328–352. https://doi.org/10.1016/J.GEOTHERMICS.2014.07.009

Huismans, R. S., Podladchikov, Y. Y., & Cloetingh, S. (2001). Dynamic modeling of the transition from passive to active rifting, application to the Pannonian Basin. *Tectonics*, *20*(6), 1021–1039. https://doi.org/10.1029/2001TC900010

IRIS (2018). Data Services Products: EMC-CAM2016 Global upper mantle surface wave tomography model. Incorporated Research Institutions for Seismology. https://doi.org/10.17611/DP/EMCCAM2016

Irvine, T. N. (1979). Rocks whose composition is determined by crystal accumulation and sorting. In H. S. Yoder (Ed.), *Evolution of the igneous rocks: Fiftieth anniversary perspectives* (pp. 245–306). Princeton, NJ: Princeton University Press.

Ivan, P., & Hovorka, D. (1993). Geochemistry and petrology of the Late Cenozoic alkali basalts of the western Carpathians (Czechoslovakia). *Mineralogy and Petrology*, *48*(1), 3–16. https://doi.org/10.1007/BF01164905

Jankovics, M. E., Harangi, S., Németh, K., Kiss, B., & Ntaflos, T. (2015). A complex magmatic system beneath the Kissomlyó monogenetic volcano (western Pannonian Basin): Evidence from mineral textures, zoning and chemistry. *Journal of Volcanology and Geothermal Research*, *301*, 38–55. https://doi.org/10.1016/j.jvolgeores.2015.04.010

Jankovics, M. E., Sági, T., Astbury, R. L., Petrelli, M., Kiss, B., Ubide, T., et al. (2019). Olivine major and trace element compositions coupled with spinel chemistry to unravel the magmatic systems feeding monogenetic basaltic volcanoes. *Journal of Volcanology and Geothermal Research*, *369*, 203–223. https://doi.org/10.1016/j.jvolgeores.2018.11.027

Jennings, E. S., & Holland, T. J. B. (2015). A simple thermodynamic model for melting of peridotite in the system NCFMASOCr. *Journal of Petrology*, *56*(5), 869–892. https://doi.org/10.1093/petrology/egv020

Johnson, K. T. M. (1998). Experimental determination of partition coefficients for rare earth and high-field-strength elements between clinopyroxene, garnet, and basaltic melt at high pressures. *Contributions to Mineralogy and Petrology*, *133*(1–2), 60–68. https://doi.org/10.1007/s004100050437

Jolivet, L., & Brun, J.-P. (2010). Cenozoic geodynamic evolution of the Aegean. *International Journal of Earth Sciences*, *99*(1), 109–138. https://doi.org/10.1007/s00531-008-0366-4

Jull, M., & McKenzie, D. (1996). The effect of deglaciation on mantle melting beneath Iceland. *Journal of Geophysical Research*, *101*(B10), 21,815–21,828. https://doi.org/10.1029/96JB01308

Katz, R. F., Spiegelman, M., & Langmuir, C. H. (2003). A new parameterization of hydrous mantle melting. *Geochemistry, Geophysics, Geosystems*, *4*(9), 1073. https://doi.org/10.1029/2002GC000433

King, S. D., & Anderson, D. L. (1995). An alternative mechanism of flood basalt formation. *Earth and Planetary Science Letters*, *136*(3–4), 269–279. https://doi.org/10.1016/0012-821X(95)00205-Q

King, S. D., & Anderson, D. L. (1998). Edge-driven convection. *Earth and Planetary Science Letters*, *160*(3–4), 289–296. https://doi.org/10.1016/S0012-821X(98)00089-2

King, S. D., & Ritsema, J. (2000). African hot spot volcanism: Small-scale convection in the upper mantle beneath cratons. *Science*, *290*(5494), 1137–1140. https://doi.org/10.1126/science.290.5494.1137

Klemme, S., & O'Neill, H. S. (2000). The near-solidus transition from garnet lherzolite to spinel lherzolite. *Contributions to Mineralogy and Petrology*, *138*(3), 237–248. https://doi.org/10.1007/s004100050560

Klöcking, M. (2018). Continental magmatism and dynamic topography (Doctoral dissertation). Cambridge, UK: University of Cambridge. https://doi.org/10.17863/CAM.18741

Klöcking, M., White, N. J., Maclennan, J., McKenzie, D., & Fitton, J. G. (2018). Quantitative relationships between basalt geochemistry, shear wave velocity, and asthenospheric temperature beneath western North America. *Geochemistry, Geophysics, Geosystems*, *19*, 3376–3404. https://doi.org/10.1029/2018GC007559

Kokfelt, T. F., Hoernle, K., & Hauff, F. (2003). Upwelling and melting of the Iceland plume from radial variation of 238U-230Th disequilibria in postglacial volcanic rocks. *Earth and Planetary Science Letters*, *214*(1–2), 167–186. https://doi.org/10.1016/S0012-821X(03)00306-6

Kovács, I., Patkó, L., Liptai, N., Lange, T., Taracsák, Z., Cloetingh, S. A. P. L., et al. (2020). The role of water and compression in the genesis of alkaline basalts: Inferences from the Carpathian-Pannonian region. *Lithos*, *354–355*, 105323. https://doi.org/10.1016/j.lithos.2019.105323

Lange, T. P., Szabó, C., Liptai, N., Patkó, L., Gelencsér, O., Aradi, L. E., & Kovács, I. J. (2019). Rheology study on the Earth's mantle: Application of quantitative Fourier transform infrared spectroscopy on upper mantle xenolith from the Perşani Mountains [in Hungarian]. *Földtani Közlöny*, *149*(3), 233. https://doi.org/10.23928/foldt.kozl.2019.149.3.233

Le Bas, M. J., Le Maitre, R. W., Streckeisen, A., & Zanettin, B. (1986). A chemical classification of volcanic rocks based on the total alkali-silica diagram. *Journal of Petrology*, *27*(3), 745–750. https://doi.org/10.1093/petrology/27.3.745

Liang, Y., & Peng, Q. (2010). Non-modal melting in an upwelling mantle column: Steady-state models with applications to REE depletion in abyssal peridotites and the dynamics of melt migration in the mantle. *Geochimica et Cosmochimica Acta*, *74*(1), 321–339. https://doi.org/10.1016/j.gca.2009.09.029

Liptai, N., Patkó, L., Kovács, I. J., Hidas, K., Pintér, Z., Jeffries, T., et al. (2017). Multiple metasomatism beneath the Nógád-Gömör volcanic field (northern Pannonian Basin) revealed by upper mantle peridotite xenoliths. *Journal of Petrology*, *58*(6), 1107–1144. https://doi.org/10.1093/petrology/egx048

Long, X., Ballmer, M. D., Córdoba, A. M. C., & Li, C. F. (2019). Mantle melting and intraplate volcanism due to self-buoyant hydrous upwellings from the stagnant slab that are conveyed by small-scale convection. *Geochemistry, Geophysics, Geosystems*, *20*, 4972–4997. https://doi.org/10.1029/2019GC008591

Mallmann, G., & O'Neill, H. S. (2009). The crystal/melt partitioning of V during mantle melting as a function of oxygen fugacity compared with some other elements (Al, P, Ca, Sc, Ti, Cr, Fe, Ga, Y, Zr and Nb). *Journal of Petrology*, *50*(9), 1765–1794. https://doi.org/10.1093/petrology/egp053

Martin, M., Wenzel, F., & CALIXTO working group (2006). High-resolution teleseismic body wave tomography beneath SE-Romania - II. Imaging of a slab detachment scenario. *Geophysical Journal International*, *164*(3), 579–595. https://doi.org/10.1111/j.1365-246X.2006.02884.x

McDonough, W. F., & Sun, S.-s. (1995). The composition of the Earth. *Chemical Geology*, *120*(3–4), 223–253. https://doi.org/10.1016/0009-2541(94)00140-4

McKenzie, D. (1985). The extraction of magma from the crust and mantle. *Earth and Planetary Science Letters*, *74*(1), 81–91. https://doi.org/10.1016/0012-821X(85)90168-2

McKenzie, D. (2020). Speculations on the generation and movement of komatiites. *Journal of Petrology*, egaa061. https://doi.org/10.1093/petrology/egaa061

McKenzie, D., & Bickle, M. J. (1988). The volume and composition of melt generated by extension of the lithosphere. *Journal of Petrology*, *29*(3), 625–679. https://doi.org/10.1093/petrology/29.3.625

McKenzie, D., & Blundy, J. (1999). Partial melt distributions from inversions with D=D(P,T,X). *AGU Abstracts*, *32*, 1021–1091. F112. V21D–07.

McKenzie, D., Jackson, J., & Priestley, K. (2019). Continental collisions and the origin of subcrustal continental earthquakes. *Canadian Journal of Earth Sciences*, *56*(11), 1101–1118. https://doi.org/10.1139/cjes-2018-0289

McKenzie, D., & O'Nions, R. K. (1991). Partial melt coefficients from inversion of rare earth element concentrations. *Journal of Petrology*, *32*(5), 1021–1091. https://doi.org/10.1093/petrology/32.5.1021

McKenzie, D., & O'Nions, R. K. (1992). Corrections to "Partial melt distributions from inversion of rare earth element concentrations". *Journal of Petrology*, *33*(6), 1453–1453. https://doi.org/10.1093/petrology/33.6.1453

McKenzie, D., & O'Nions, R. K. (1995). The source regions of ocean island basalts. *Journal of Petrology*, *36*(1), 133–159. https://doi.org/10.1093/petrology/36.1.133

McNab, F., Ball, P. W., Hoggard, M. J., & White, N. J. (2018). Neogene uplift and magmatism of Anatolia: Insights from drainage analysis and basaltic geochemistry. *Geochemistry, Geophysics, Geosystems*, *19*, 175–213. https://doi.org/10.1002/2017GC007251

Miyashiro, A. (1978). Nature of alkalic volcanic rock series. *Contributions to Mineralogy and Petrology*, *66*(1), 91–104. https://doi.org/10.1007/BF00376089

Morgan, W. J. (1971). Convection plumes in the lower mantle. *Nature*, *230*(5288), 42–43. https://doi.org/10.1038/230042a0

Ntaflos, T., Bizimis, M., & Abart, R. (2017). Mantle xenoliths from Szentbékálla, Balaton: Geochemical and petrological constraints on the evolution of the lithospheric mantle underneath Pannonian Basin, Hungary. *Lithos*, *276*, 30–44. https://doi.org/10.1016/j.lithos.2016.12.018

Patkó, L., Liptai, N., Aradi, L. E., Klébesz, R., Sendula, E., Bodnar, R. J., et al. (2020). Metasomatism-induced wehrlite formation in the upper mantle beneath the Nógrád-Gömör volcanic field (Northern Pannonian Basin): Evidence from xenoliths. *Geoscience Frontiers*, *11*(3), 943–964. https://doi.org/10.1016/j.gsf.2019.09.012

Patkó, L., Liptai, N., Kovács, I. J., Aradi, L. E., Xia, Q.-K., Ingrin, J., et al. (2019). Extremely low structural hydroxyl contents in upper mantle xenoliths from the Nógrád-Gömör volcanic field (northern Pannonian Basin): Geodynamic implications and the role of post-eruptive re-equilibration. *Chemical Geology*, *507*, 23–41. https://doi.org/10.1016/J.CHEMGEO.2018.12.017

Pearce, J. A., & Peate, D. W. (1995). Tectonic implications of the composition of volcanic arc magmas. *Annual Review of Earth and Planetary Sciences*, *23*(1), 251–285. https://doi.org/10.1146/annurev.ea.23.050195.001343

Pécskay, Z., Lexa, J., Szakács, A., Seghedi, I., Balogh, K., Konečný, V., et al. (2006). Geochronology of Neogene magmatism in the Carpathian arc and intra-Carpathian area. *Geologica Carpathica*, *57*(6), 511–530.

Plank, T., & Forsyth, D. W. (2016). Thermal structure and melting conditions in the mantle beneath the Basin and Range province from seismology and petrology. *Geochemistry, Geophysics, Geosystems*, *17*, 1312–1338. https://doi.org/10.1002/2015GC006205

Priestley, K., & McKenzie, D. (2013). The relationship between shear wave velocity, temperature, attenuation and viscosity in the shallow part of the mantle. *Earth and Planetary Science Letters*, *381*, 78–91. https://doi.org/10.1016/j.epsl.2013.08.022

Priestley, K., McKenzie, D., & Ho, T. (2018). A lithosphere-asthenosphere boundary - global model derived from multimode surface-wave tomography and petrology. In H. Yuan & B. Romanowicz (Eds.), *Lithospheric discontinuities*, *Geophysical Monograph Series* (Vol. 239, pp. 111–123). Washington, DC: American Geophysical Union (AGU). https://doi.org/10.1002/9781119249740.ch6

Richards, M. A., Duncan, R. A., & Courtillot, V. E. (1989). Flood basalts and hot-spot tracks: Plume heads and tails. *Science*, *246*(4926), 103–107. https://doi.org/10.1126/science.246.4926.103

Rosenbaum, J. M., Wilson, M., & Downes, H. (1997). Multiple enrichment of the Carpathian-Pannonian mantle: Pb-Sr-Nd isotope and trace element constraints. *Journal of Geophysical Research*, *102*(B7), 14,947–14,961. https://doi.org/10.1029/97JB01037

Royden, L. H. (1988). Late Cenozoic tectonics of the Pannonian Basin system. In L. H. Royden & F. Horváth (Eds.), *The Pannonian Basin: A study in basin evolution*, *AAPG Memoirs* (Vol. 45, pp. 27–48). Tulsa, OK: American Association of Petroleum Geologists (AAPG). https://doi.org/10.1306/M45474C3

Schmid, S. M., Fügenschuh, B., Kounov, A., Matenco, L., Nievergelt, P., Oberhänsli, R., et al. (2020). Tectonic units of the Alpine collision zone between Eastern Alps and western Turkey. *Gondwana Research*, *78*, 308–374. https://doi.org/10.1016/j.gr.2019.07.005

Seghedi, I., Downes, H., Vaselli, O., Szakács, A., Balogh, K., & Pécskay, Z. (2004). Post-collisional Tertiary-Quaternary mafic alkalic magmatism in the Carpathian-Pannonian region: A review. *Tectonophysics*, *393*(1–4), 43–62. https://doi.org/10.1016/J.TECTO.2004.07.051

Seghedi, I., Maţenco, L., Downes, H., Mason, P. R. D., Szakács, A., & Pécskay, Z. (2011). Tectonic significance of changes in post-subduction Pliocene-Quaternary magmatism in the south east part of the Carpathian-Pannonian Region. *Tectonophysics*, *502*(1–2), 146–157. https://doi.org/10.1016/j.tecto.2009.12.003

Seghedi, I., Popa, R.-G., Panaiotu, C. G., Szakács, A., & Pécskay, Z. (2016). Short-lived eruptive episodes during the construction of a Na-alkalic basaltic field (Perşani Mountains, SE Transylvania, Romania). *Bulletin of Volcanology*, *78*(10), 69. https://doi.org/10.1007/s00445-016-1063-y

Shako, R., Förste, C., Abrikosov, O., Bruinsma, S., Marty, J.-C., Lemoine, J.-M., et al. (2014). EIGEN-6C: A high-resolution global gravity combination model including GOCE data. In F. Flechtner, F. Sneeuw, & W. D. Schuh (Eds.), *Observation of the system Earth from space - CHAMP, GRACE, GOCE and future missions. Advanced technologies in Earth sciences* (pp. 155–161). Heidelberg: Springer, Berlin. https://doi.org/10.1007/978-3-642-32135-1_20

Shannon, R. D. (1976). Revised effective ionic radii and systematic studies of interatomic distances in halides and chalcogenides. *Acta Crystallographica Section A*, *32*(5), 751–767. https://doi.org/10.1107/S0567739476001551

Slater, L., McKenzie, D., Grönvold, K., & Shimizu, N. (2001). Melt generation and movement beneath Theistareykir, NE Iceland. *Journal of Petrology*, *42*(2), 321–354. https://doi.org/10.1093/petrology/42.2.321

Smith, W. H. F., & Sandwell, D. T. (1997). Global sea floor topography from satellite altimetry and ship depth soundings. *Science*, *277*(5334), 1956–1962. https://doi.org/10.1126/science.277.5334.1956

Stracke, A., Bizimis, M., & Salters, V. J. M. (2003). Recycling oceanic crust: Quantitative constraints. *Geochemistry, Geophysics, Geosystems*, *4*(3), 8003. https://doi.org/10.1029/2001GC000223

Sun, S.-s., & McDonough, W. F. (1989). Chemical and isotopic systematics of oceanic basalts: Implications for mantle composition and processes. *Geological Society, London, Special Publications*, *42*(1), 313–345. http://dx.doi.org/10.1144/gsl.sp.1989.042.01.19

Szabó, C., Bodnar, R. J., & Sobolev, A. V. (1996). Metasomatism associated with subduction-related, volatile-rich silicate melt in the upper mantle beneath the Nógrád-Gömör volcanic field, northern Hungary/southern Slovakia: Evidence from silicate melt inclusions. *European Journal of Mineralogy*, *8*(5), 881–899.

Szabó, C., Falus, G., Zajacz, Z., Kovács, I., & Bali, E. (2004). Composition and evolution of lithosphere beneath the Carpathian-Pannonian Region: A review. *Tectonophysics*, *393*(1–4), 119–137. https://doi.org/10.1016/j.tecto.2004.07.031

Szabó, C., & Taylor, L. A. (1994). Mantle petrology and geochemistry beneath the Nógrád-Gömör volcanic field, Carpathian-Pannonian region. *International Geology Review*, *36*(4), 328–358. https://doi.org/10.1080/00206819409465465

Szabó, C., Vaselli, O., Vannucci, R., Bottazzi, P., Ottolini, L., Coradossi, N., & Kubovics, I. (1995). Ultramafic xenoliths from the Little Hungarian Plain (western Hungary): A petrologic and geochemical study. *Acta Vulcanologica*, *7*(2), 249–263.

Tschegg, C., Ntaflos, T., Kiraly, F., & Harangi, S. (2010). High temperature corrosion of olivine phenocrysts in Pliocene basalts from Banat, Romania. *Austrian Journal of Earth Sciences*, *103*(1), 101–110.

Ustaszewski, K., Schmid, S. M., Fügenschuh, B., Tischler, M., Kissling, E., & Spakman, W. (2008). A map-view restoration of the Alpine-Carpathian-Dinaridic system for the Early Miocene. *Swiss Journal of Geosciences*, *101*(1), S273–S294. https://doi.org/10.1007/s00015-008-1288-7

Vaselli, O., Downes, H., Thirlwall, M., Dobosi, G., Coradossi, N., Seghedi, I., et al. (1995). Ultramafic xenoliths in Plio-Pleistocene alkali basalts from the eastern Transylvanian Basin: Depleted mantle enriched by vein metasomatism. *Journal of Petrology*, *36*(1), 23–53. https://doi.org/10.1093/petrology/36.1.23

Vaselli, O., Downes, H., Thirlwall, M. F., Vannucci, R., & Coradossi, N. (1996). Spinel-peridotite xenoliths from Kapfenstein (Graz Basin, Eastern Austria): A geochemical and petrological study. *Mineralogy and Petrology*, *57*(1–2), 23–50. https://doi.org/10.1007/BF01161620

Veksler, I. V., Petibon, C., Jenner, G. A., Dorfman, A. M., & Dingwell, D. B. (1998). Trace element partitioning in immiscible silicate-carbonate liquid systems: An initial experimental study using a centrifuge autoclave. *Journal of Petrology*, *39*(11–12), 2095–2104.

White, R. S., & McKenzie, D. (1995). Mantle plumes and flood basalts. *Journal of Geophysical Research*, *100*(B9), 17,543–17,585. https://doi.org/10.1029/95JB01585

Willbold, M., & Stracke, A. (2006). Trace element composition of mantle end-members: Implications for recycling of oceanic and upper and lower continental crust. *Geochemistry, Geophysics, Geosystems*, *7*, Q04004. https://doi.org/10.1029/2005GC001005

Wilson, M., & Downes, H. (1991). Tertiary–Quaternary extension-related alkaline magmatism in western and central Europe. *Journal of Petrology*, *32*(4), 811–849. https://doi.org/10.1093/petrology/32.4.811

Wood, B. J., & Blundy, J. D. (1997). A predictive model for rare earth element partitioning between clinopyroxene and anhydrous silicate melt. *Contributions to Mineralogy and Petrology*, *129*(2–3), 166–181. https://doi.org/10.1007/s004100050330

Workman, R. K., & Hart, S. R. (2005). Major and trace element composition of the depleted MORB mantle (DMM). *Earth and Planetary Science Letters*, *231*(1–2), 53–72. https://doi.org/10.1016/j.epsl.2004.12.005

Wortel, M. J. R., & Spakman, W. (2000). Subduction and slab detachment in the Mediterranean-Carpathian region. *Science*, *290*(5498), 1910–1917. https://doi.org/10.1126/science.290.5498.1910

Yang, J., & Faccenda, M. (2020). Intraplate volcanism originating from upwelling hydrous mantle transition zone. *Nature*, *579*(7797), 88–91. https://doi.org/10.1038/s41586-020-2045-y

Zelenka, T., Balázs, E., Balogh, K., Kiss, J., Kozák, M., Nemesi, L., et al. (2004). Buried Neogene volcanic structures in Hungary. *Acta Geologica Hungarica*, *47*(2–3), 177–219. https://doi.org/10.1556/AGeol.47.2004.2-3.6